nature aging

Article

https://doi.org/10.1038/s43587-023-00560-5

Prophylactic and long-lasting efficacy of senolytic CAR T cells against age-related metabolic dysfunction

Received: 31 January 2023

Accepted: 18 December 2023

Published online: 24 January 2024

Check for updates

Corina Amor[1,14] ✉, Inés Fernández-Maestre[2,3,14], Saria Chowdhury[1], Yu-Jui Ho[4], Sandeep Nadella[1], Courtenay Graham[5], Sebastian E. Carrasco[6], Emmanuella Nnuji-John[1,7], Judith Feucht[8,9], Clemens Hinterleitner[4], Valentin J. A. Barthet[4], Jacob A. Boyer[10,11], Riccardo Mezzadra[4], Matthew G. Wereski[2], David A. Tuveson[1], Ross L. Levine[2,12], Lee W. Jones[5,12], Michel Sadelain[8] & Scott W. Lowe[4,13]

Senescent cells, which accumulate in organisms over time, contribute to age-related tissue decline. Genetic ablation of senescent cells can ameliorate various age-related pathologies, including metabolic dysfunction and decreased physical fitness. While small-molecule drugs that eliminate senescent cells ('senolytics') partially replicate these phenotypes, they require continuous administration. We have developed a senolytic therapy based on chimeric antigen receptor (CAR) T cells targeting the senescence-associated protein urokinase plasminogen activator receptor (uPAR), and we previously showed these can safely eliminate senescent cells in young animals. We now show that uPAR-positive senescent cells accumulate during aging and that they can be safely targeted with senolytic CAR T cells. Treatment with anti-uPAR CAR T cells improves exercise capacity in physiological aging, and it ameliorates metabolic dysfunction (for example, improving glucose tolerance) in aged mice and in mice on a high-fat diet. Importantly, a single administration of these senolytic CAR T cells is sufficient to achieve long-term therapeutic and preventive effects.

Cellular senescence is a stress response program characterized by stable cell cycle arrest[1,2] and the production of the senescence-associated secretory phenotype (SASP), which includes pro-inflammatory cytokines and matrix remodeling enzymes[3]. In physiological conditions in young individuals (for example, wound healing, tumor suppression), the SASP contributes to the recruitment of immune cells, whose role is to clear the senescent cells and facilitate restoration of tissue homeostasis[3]. However, during aging, the combination of increased tissue

[1]Cold Spring Harbor Laboratory, Cold Spring Harbor, NY, USA. [2]Human Oncology and Pathogenesis Program, Memorial Sloan Kettering Cancer Center, New York, NY, USA. [3]Louis V. Gerstner Jr Graduate School of Biomedical Sciences, Memorial Sloan Kettering Cancer Center, New York, NY, USA. [4]Department of Cancer Biology and Genetics. Memorial Sloan Kettering Cancer Center, New York, NY, USA. [5]Department of Medicine, Memorial Sloan Kettering Cancer Center, New York, NY, USA. [6]Laboratory of Comparative Pathology. Weill Cornell Medicine, Memorial Sloan Kettering Cancer Center, and Rockefeller University, New York, NY, USA. [7]Cold Spring Harbor School of Biological Sciences, Cold Spring Harbor, NY, USA. [8]Center for Cell Engineering, Memorial Sloan Kettering Cancer Center, New York, NY, USA. [9]Cluster of Excellence iFIT, University Children's Hospital Tuebingen, Tuebingen, Germany. [10]Lewis Sigler Institute for Integrative Genomics and Department of Chemistry, Princeton University, Princeton, NJ, USA. [11]Ludwig Institute for Cancer Research, Princeton Branch, Princeton, NJ, USA. [12]Department of Medicine, Weill Cornell Medical College, New York, NY, USA. [13]Howard Hughes Medical Institute, Memorial Sloan Kettering Cancer Center, New York, NY, USA. [14]These authors contributed equally: Corina Amor, Inés Fernández-Maestre. ✉e-mail: amor@cshl.edu

damage and decreased function of the immune system leads to the accumulation of senescent cells[4,5], thereby generating a chronic pro-inflammatory milieu that leads to a range of age-related tissue pathologies[6–9]. As such, senolytic strategies to eliminate senescent cells from aged tissues have the potential to dramatically improve healthspan.

Most efforts to develop senolytic therapies have focused on the development of small-molecule drugs that target poorly defined molecular dependencies present in senescent cells and that must be administered repeatedly over time[10]. In contrast, CAR T cells are a form of cellular therapy that redirects T cell specificity toward cells expressing a specific cell-surface antigen[11]. Unlike small molecules, CAR T cells only require that the target antigen is differentially expressed on target cells compared to normal tissues; moreover, as 'living drugs', these therapeutics have the potential to persist and mediate their potent effects for years after single administration[12]. We have shown that CAR T cells targeting the cell-surface protein uPAR, which is upregulated on senescent cells, can efficiently deplete senescent cells in young animals and reverse liver fibrosis. Here, we explore whether CAR T cells could safely and effectively eliminate senescent cells in aged mice and modulate healthspan.

Results

uPAR is upregulated in physiological aging

uPAR promotes remodeling of the extracellular matrix during fibrinolysis, wound healing and tumorigenesis[13]. In physiological conditions, it is primarily expressed in certain subsets of myeloid cells and, at low levels, in the bronchial epithelium[14]. We recently described the upregulation of uPAR on senescent cells across different cell types and multiple triggers of senescence[14] and showed that CAR T cells targeting this cell-surface protein could efficiently remove senescent cells from tissues in young mice without deleterious effects to normal tissues[14]. Given these results, we set out to test whether uPAR might serve as a target for senolytic CAR T cells in aged tissues.

Plasma levels of soluble uPAR positively correlate with the pace of aging in humans[15,16] and *Plaur* (the gene encoding uPAR) is a component of the SenMayo gene signature recently reported to identify senescent cells in aged tissues[17]. To explore the association with uPAR expression in aged tissues further, we surveyed RNA-sequencing (RNA-seq) data from the Tabula Muris Senis project[18]. Expression of *Plaur* was upregulated in several organs in samples from 20-month-old mice compared to 3-month-old mice (Extended Data Fig. 1a). Because mRNA levels are not linearly related to surface protein levels[19], we performed immunohistochemistry and indeed confirmed an age-associated increase in uPAR protein in liver, adipose tissue, skeletal muscle and pancreas (Fig. 1a and Extended Data Fig. 1b). This increase in the fraction of uPAR-positive cells was paralleled by an increase in the percentage of senescence-associated beta-galactosidase (SA-β-gal)-positive cells (Extended Data Fig. 1c–f). Co-immunofluorescence revealed that a large majority of these SA-β-gal-expressing cells were in fact uPAR positive, whereas only a minority of these cells were macrophages as evidenced by coexpression of F4/80 (Extended Data Fig. 1g–j).

To add granularity to our understanding of the molecular characteristics of uPAR-positive cells in aged tissues, we performed single-cell RNA sequencing (scRNA-seq) on approximately 4,000–15,000 uPAR-positive and uPAR-negative cells sorted by fluorescence-activated cell sorting (FACS) from the liver, fat and pancreas (Fig. 1b–m and Extended Data Figs. 2 and 3). Using unsupervised clustering and marker-based cell labeling[20,21], we identified the major uPAR-positive cell types and cell states present in each of the three organs (Fig. 1b–d and Extended Data Fig. 2). Of note, some minor cell types (for example, hepatic stellate cells in the liver, and beta cells in the pancreas) require specialized isolation procedures and were not captured using our protocol[22,23].

Analysis of the different populations for uPAR expression indicated that endothelial and myeloid cells were the most prominent uPAR-expressing populations in the liver (Fig. 1e and Extended Data Fig. 2b), whereas in adipose tissue uPAR was expressed mainly in subsets of preadipocytes, dendritic cells and myeloid cells (Fig. 1f and Extended Data Fig. 2d). In the aged pancreas, uPAR expression was prominent in subsets of endothelial cells, fibroblasts, dendritic cells and myeloid cells (Fig. 1g and Extended Data Fig. 2f). Compared to uPAR-negative cells, uPAR-positive cells were significantly enriched in gene signatures linked to inflammation, the complement pathway and the coagulation cascade as well as transforming growth factor-beta signaling (Extended Data Fig. 3a–c).

Importantly, when senescent cells present in these tissues were identified using two independent transcriptomic signatures of senescence[17,24], we observed that the main senescent cell types present in aged tissues were distinct: endothelial and myeloid cells in the liver (Fig. 1h and Extended Data Fig. 3d,g–i), dendritic cells, myeloid cells and preadipocytes in adipose tissue (Fig. 1j and Extended Data Fig. 3e,j–l) and endothelial cells, fibroblasts, dendritic cells and myeloid cells in the pancreas (Fig. 1l and Extended Data Fig. 3f,m–o). Thus, uPAR-positive cells constituted a significant fraction of the senescent cell burden in these tissues (67–90% in liver, 92–66% in adipose tissue and 76–63% in pancreas; Fig. 1i,k,m and Extended Data Fig. 3h,k,n). Note that while our analysis could not evaluate pancreatic beta cells, analysis of published data revealed that expression of *Plaur* was significantly upregulated in senescent beta cell populations isolated from aged animals and subjected to bulk RNA-seq[25].

Finally, to ascertain whether uPAR was expressed in senescent cells that accumulate with age in human tissues, we analyzed available datasets of human pancreas collected from young (0- to 6-year-old) and aged (50- to 76-year-old) individuals[26]. While we were limited to an analysis of *PLAUR* transcript abundance in these settings, we found that the fraction of *PLAUR*-expressing cells was substantially greater in older individuals (Fig. 2).

Overall, these results indicate that the levels of uPAR-positive senescent cells increase with age and that most senescent cells present in aged tissues express uPAR. The fact that we can identify settings in which an increased expression of uPAR protein expression does not correlate with *Plaur* mRNA levels indicates that the absence of an induction of *Plaur* transcript levels does not exclude the possibility of an increase in uPAR protein expression.

Effect of uPAR CAR T cells in naturally aged mice

To determine the tolerability and therapeutic activity of uPAR-targeting CAR T cells on physiologically aged mice, we intravenously infused

Fig. 1 | uPAR is upregulated on senescent cells in physiological aging. **a**, Immunohistochemical staining of mouse uPAR in liver, adipose tissue, muscle and pancreas from young (age 3 months) or old (age 20 months) mice ($n = 3$ per age). **b**–**m**, Single-cell analysis of uPAR expression and senescence. uPAR-positive and uPAR-negative cells were sorted from the liver, adipose tissue and pancreas of 20-month-old mice and subjected to single-cell RNA-seq by 10x chromium protocol (n = the sequencing of four mice where two females were combined into one replicate and two males were combined into another replicate). **b**, Uniform manifold approximation and projection (UMAP) visualization of liver cell types. **c**, UMAP visualization of adipose tissue cell types. **d**, UMAP visualization of pancreas cell types. **e**, UMAP visualization of hepatic uPAR-negative and uPAR-positive cell types. **f**, UMAP visualization of adipose uPAR-negative and uPAR-positive cell types. **g**, UMAP visualization of pancreatic uPAR-negative and uPAR-positive cell types. **h**,**j**,**l**, UMAP visualizations with senescence signature scores[24] in each cell indicated by the color scale. **i**,**k**,**m**, Quantification of the proportion of uPAR-positive and uPAR-negative cells contributing to the respective senescence signature. **h**,**i**, Liver; **j**,**k**, adipose tissue; **l**,**m**, pancreas. Results are from one independent experiment (**a**–**m**). DC, dendritic cell; NK, natural killer; pDC, plasmacytoid dendritic cell; ASPC, adipose progenitor and stem cells.

https://doi.org/10.1038/s43587-023-00560-5

aged C57BL/6 mice (18–20 months old) with our previously developed mouse second-generation CAR T cells targeting mouse uPAR[14] (m.uPAR-m.28z). m.uPAR-m.28z CAR T cells contain an anti-mouse uPAR single-chain variable fragment (scFV) linked to mouse CD28 costimulatory and mouse CD3ζ signaling domains and are, therefore, fully mouse CAR T cells that allow for syngeneic studies[14]. Importantly, the CAR T cells were generated from CD45.1 mice and infused into C57BL/6 mice, which are CD45.2, thus allowing for CAR T cells to be differentiated from

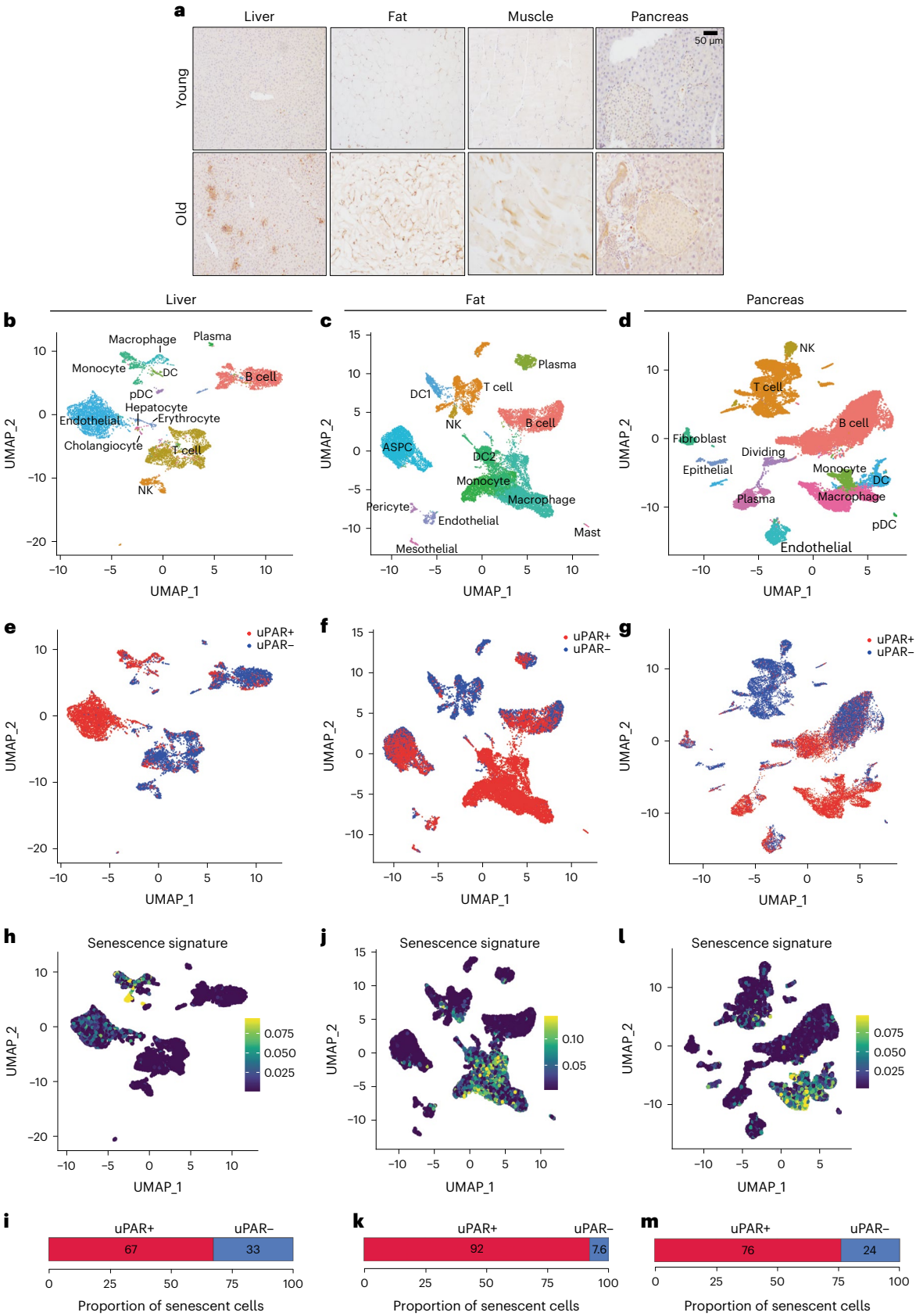

https://doi.org/10.1038/s43587-023-00560-5

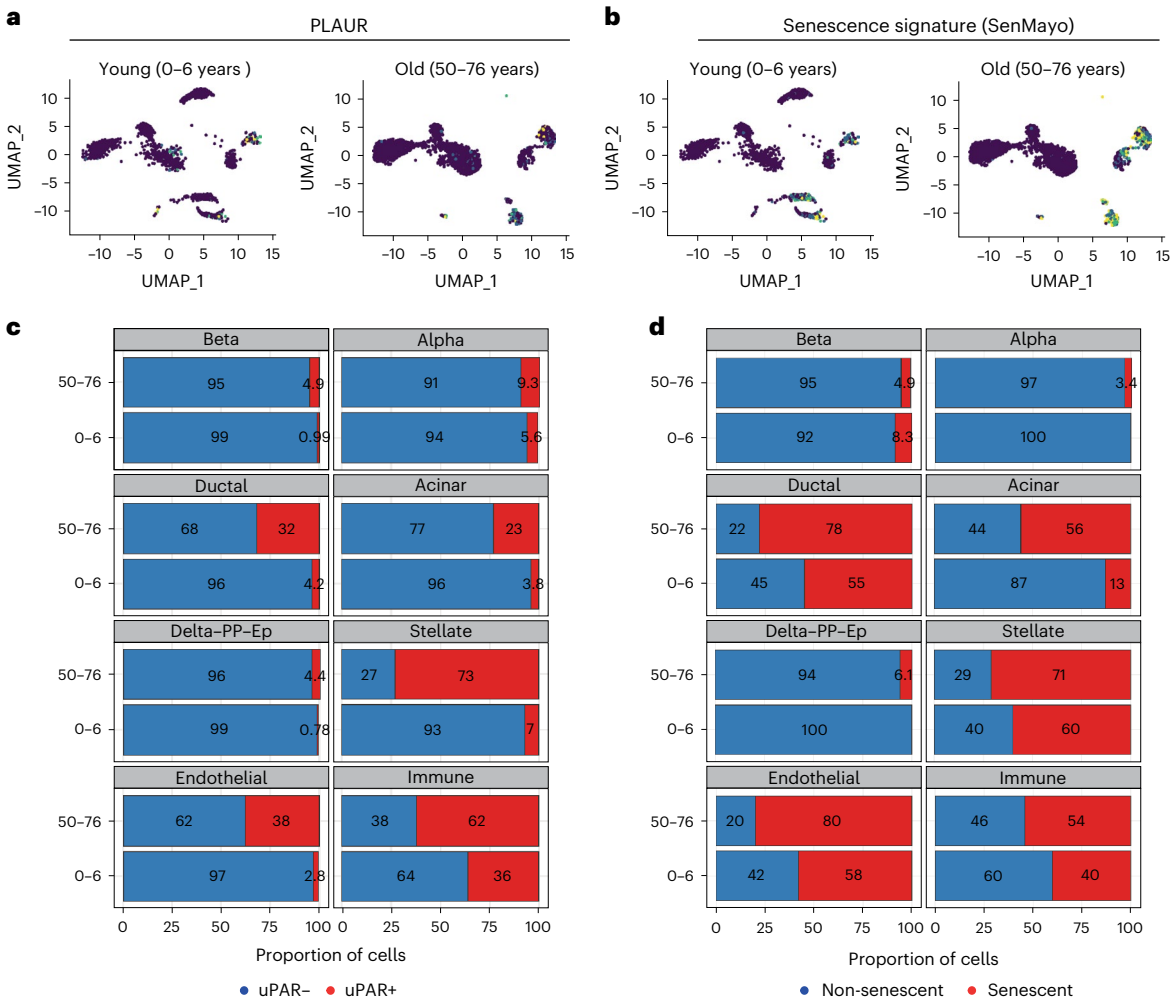

Fig. 2 | Upregulation of uPAR and senescence signatures in aged human pancreas. scRNA-seq data of human pancreas of different ages from ref. 26 were analyzed. **a**, UMAP visualization of *Plaur* expression across pancreas cell types in young humans (0–6 years old) and old humans (50–76 years old). **b**, UMAP visualization of senescence signature expression[17] across pancreas cell types in young humans (0–6 years old) and old humans (50–76 years old). **c**, Quantification of the proportion of uPAR-positive and uPAR-negative cells by cell type and age. **d**, Quantification of the proportion of cells expressing senescence signature[17] or not expressing senescence signature[17] by cell type and age.

endogenous T cells and therefore monitored over time (Fig. 3a). As controls, parallel cohorts of sex- and aged-matched mice were infused with the same dose of either untransduced T (UT) cells or T cells expressing a mouse CAR targeting human CD19 (h.19-m.28z) that does not recognize the mouse CD19 protein but encompasses the exact same signaling structure thus controlling for nonspecific T cell cytotoxicity. We opted to test a dose of 0.5×10^6 CAR-positive cells, which we previously found to balance safety and senolytic efficacy in young animals[14].

Mice infused with m.uPAR-m.28z CAR T cells, but not controls, showed a reduction in the proportions of SA-β-gal-positive and uPAR-positive cells throughout the tissues examined, most notably in the pancreas, liver and adipose tissue (Fig. 3b and Extended Data Fig. 4). As has been previously reported, our aged mouse cohort displayed elevated levels of pro-inflammatory cytokines linked to the SASP in the peripheral blood, a phenomenon often referred to as 'inflammaging'[27]. Consistent with a reduction in senescent cell burden and/or improved organismal health, m.uPAR-m.28z CAR T cell-treated animals showed a decrease in the plasma levels of these factors (Fig. 3c).

Despite detectable expression of uPAR in some normal tissues, our previous work indicates that a dose of 0.5×10^6 m.uPAR-m.28z CAR T cells is well tolerated in young mice[14]. As was the case in young animals, the dose of 0.5×10^6 m.uPAR-m.28z CAR T cells was well tolerated in aged mice (18–20 months old), all of whom remained active without observable signs of morbidity, weight loss or relevant alterations in serum chemistry or complete blood counts (Fig. 4). In addition, microscopic evaluation of tissues did not reveal tissue damage secondary to toxicity in aged tissues obtained from whole-body necropsies of m.uPAR-m.28z CAR T cell-treated mice when compared to age-matched control-treated animals (Extended Data Fig. 5).

One prominent feature of aging in humans and mice is the emergence of age-related metabolic dysfunction, which is a collection of phenotypes linked to impaired glucose tolerance[25,28] and decreased exercise capacity[29,30]. Interestingly, we observed that aged m.uPAR-m.28z CAR T cell-treated mice had significantly decreased fasting glucose levels compared with UT or h.19-m.28z-treated controls (Fig. 5a). Upon challenge with an intraperitoneal bolus of glucose (2 g per kg body weight), m.uPAR-m.28z CAR T cell-treated aged but not young mice presented significantly lower plasma glucose levels than controls for over 2 h after administration (Fig. 5b,c and Extended Data Fig. 6a,b). Furthermore, m.uPAR-m.28z CAR T cell-treated mice had lower basal insulin levels after fasting that was followed by a significant increase in insulin levels 15 min after the glucose load, indicative of improved pancreatic beta cell function (Fig. 5d). Of note, m.uPAR-m.28z CAR T cell-treated aged mice also presented improved peripheral

https://doi.org/10.1038/s43587-023-00560-5

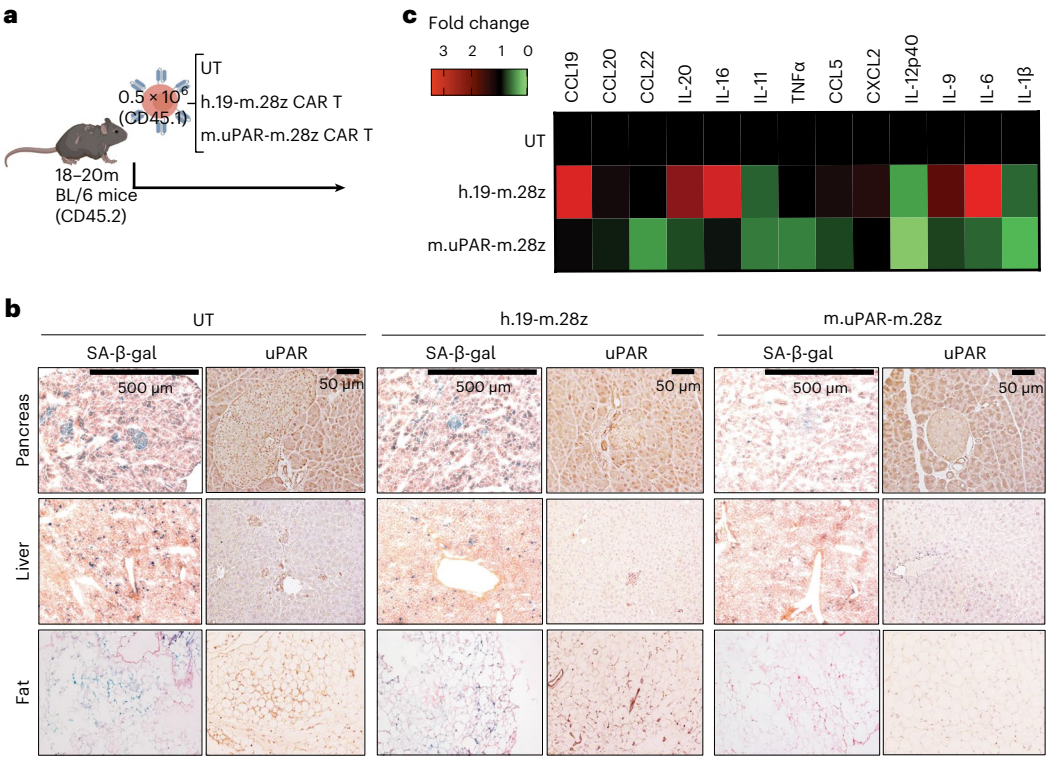

Fig. 3 | uPAR CAR T cells eliminate senescent cells in old mice. a, Experimental scheme for Figs. 3–5. C57BL/6N mice (18 to 20 months old) were injected with 0.5×10^6 m.uPAR-m.28z CAR T cells, h.19-m.28z CAR T cells or UT cells generated from CD45.1 mice 16 h after administration of cyclophosphamide (200 mg per kg body weight). Mice were harvested 20 d later and/or monitored over time. Schematic created with BioRender.com. **b**, Representative SA-β-gal and uPAR staining 20 d after cell infusion. **c**, Heat map depicting fold change in the levels of SASP cytokines compared to UT-treated mice ($n = 3$ for UT cells; $n = 3$ for h.19-m.28z; $n = 4$ for m.uPAR-m.28z). Results are from one experiment (**b** and **c**).

insulin sensitivity, suggesting a coordinated multiorgan improvement in glucose homeostasis (Extended Data Fig. 6c,d). In addition, most aged mice with m.uPAR-m.28z CAR T cells showed improvements in their exercise capacity at 2.5 months after treatment compared to pretreatment levels (Fig. 5e,f).

Importantly, the improvement in metabolic function noted in m.uPAR-m.28z CAR T cell-treated old mice was accompanied by an expansion of m.uPAR-m.28z CAR T cells and their trafficking to several organs such as liver and spleen as assessed by flow cytometry (Fig. 5g,h). These m.uPAR-m.28z CAR T cells were mostly cytotoxic $CD8^+$T cells in the livers and $CD4^+$T cells in the spleen and presented an effector phenotype indicative of their activated response (Extended Data Fig. 7a–d). Of note, this expansion did not occur in aged-matched UT or h.19-m.28z-treated controls and was lower in m.uPAR-m.28z CAR T cell-treated young mice, results that were consistent with the lower fraction of uPAR-positive cells in younger animals (Figs. 1a and 5g,h and Extended Data Fig. 1).

Collectively, these results show that uPAR CAR T cells can safely and effectively remove senescent uPAR-positive cells in the tissues of naturally aged mice and ameliorate age-dependent metabolic and physical dysfunction.

Persistence and prophylaxis by uPAR CAR T cells in aging

Unlike small molecules, CAR T cells can persist in the organism and exert their effects over time[12]. Indeed, in human cancer patients cured of disease, the presence of CAR T cells has been noted as much as 10 years after the initial infusion[12]. Such persistence raises the question of whether the administration of uPAR CAR T cells in young animals would prevent or delay the development of age-triggered phenotypes later in life. To explore this possibility, we infused young mice (3 months old) with one dose of 0.5×10^6 m.uPAR-m.28z CAR T, h.19-m.28z CAR T or UT cells and monitored the mice over their natural lifespan (Fig. 6). Despite the initially lower numbers of uPAR-positive cells compared to aged animals (see above), uPAR CAR T cells were detectable in the spleens and livers of treated mice 12 months after the initial single infusion at substantially higher levels than the low number of persisting UT or h.19 CAR T controls (Fig. 6a,b). Consistent with their persistent activity, flow cytometry of the spleen and livers of uPAR CAR T cell-treated mice indicated that the persisting cells were mostly cytotoxic $CD8^+$ T cells harboring a memory and effector phenotype in the spleens (Extended Data Fig. 7e–h). Therefore, uPAR CAR T cells persist and expand over the lifespan of the animal, presumably owing to increased antigen stimulation as the frequency of target uPAR-positive cells increases over time.

As was observed in aged animals upon therapeutic treatment, prophylactic uPAR CAR T cell administration in young mice limited metabolic decline in old age. Specifically, uPAR CAR T cell-treated mice had significantly lower fasting glucose levels (Fig. 6c), improved glucose tolerance (Fig. 6d,e) and enhanced pancreatic beta cell function as assessed by glucose-stimulated insulin secretion (Fig. 6f) than mice treated with either UT or h.19-m.28z. In terms of fitness, mice that in their youth had been treated with m.uPAR-m.28z CAR T cells, compared with control-treated mice, showed higher exercise capacity at 9 months of age (Fig. 6g,h), although this waned over time (Extended Data Fig. 7i,j). These phenotypes correlated with a significant decrease in both SA-β-gal-positive and uPAR-positive cells in pancreas, liver and adipose tissue (Fig. 6i and Extended Data Fig. 7k–p). Taken together, these results show that uPAR CAR T cells can not only treat, but also prevent, features of age-dependent metabolic decline.

uPAR CAR T cells to treat or prevent metabolic syndrome

Many of the features associated with metabolic syndrome in aged mice can be recapitulated in young animals given a high-fat diet

https://doi.org/10.1038/s43587-023-00560-5

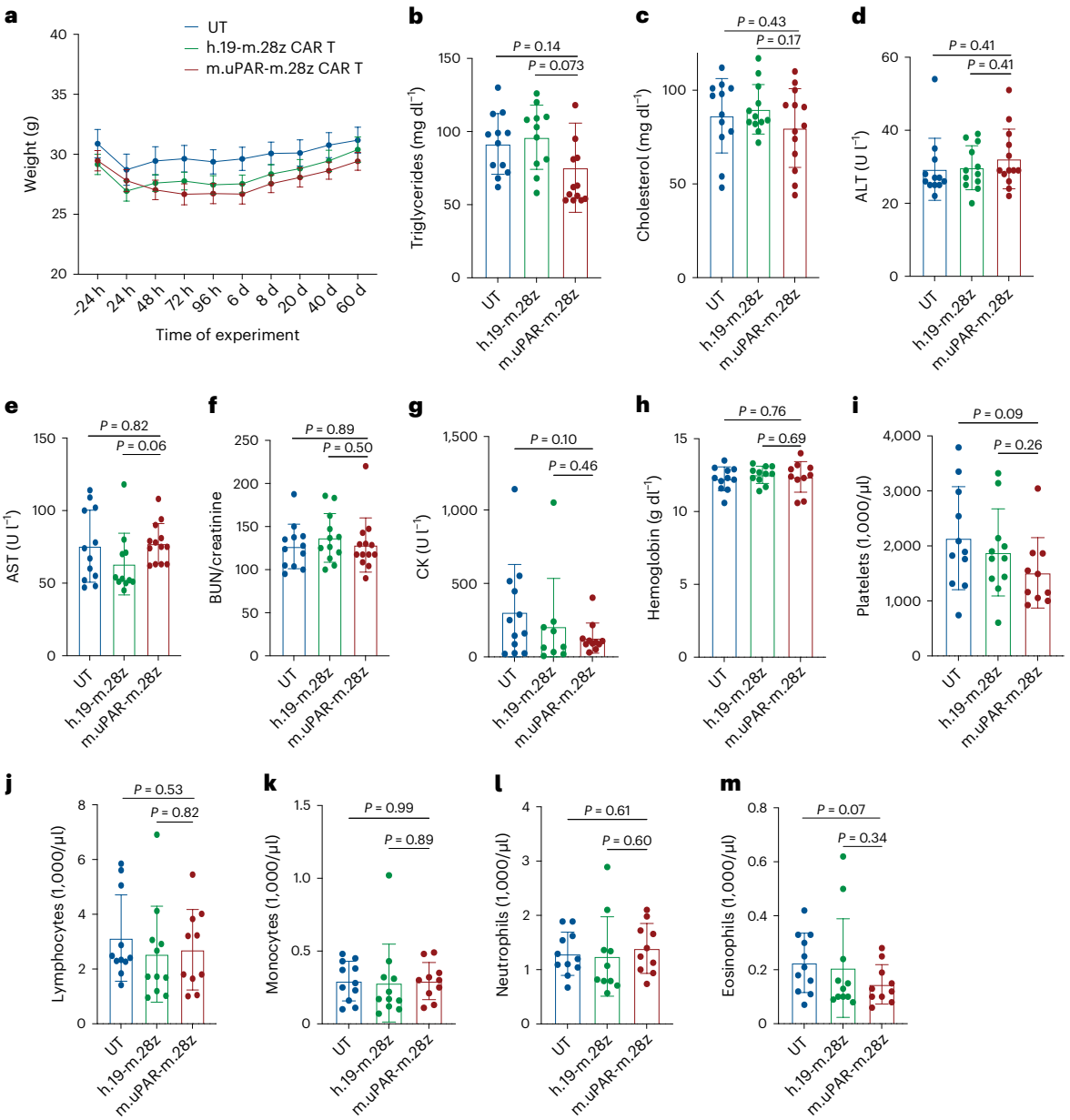

Fig. 4 | Safety of uPAR CAR T cells in aged mice. Mice were treated with m.uPAR-m.28z CAR T cells, h.19-m.28z CAR T cells or UT cells as schematized in Fig. 3a. **a**, Body weight 24 h before and at various times after cell infusion ($n = 12$ mice for UT; $n = 11$ for h.19-m.28z; $n = 12$ for m.uPAR-m.28z). **b**, Triglyceride levels 20 d after cell infusion ($n = 12$ mice for UT; $n = 11$ for h.19-m.28z; $n = 13$ for m.uPAR-m.28z). **c**, Cholesterol levels 20 d after cell infusion ($n = 12$ for UT and for h.19-m.28z; $n = 13$ for m.uPAR-m.28z). **d**, Alanine transaminase (ALT) levels 20 d after cell infusion (sample sizes as in **c**). **e**, Aspartate aminotransferase (AST) levels 20 d after cell infusion ($n = 12$ for UT; $n = 11$ for h.19-m.28z; $n = 13$ for m.uPAR-m.28z). **f**, BUN/creatinine ratio 20 d after cell infusion (sample sizes as in **c**). **g**, Creatine kinase (CK) 20 d after cell infusion ($n = 12$ for UT; $n = 9$ for h.19-m.28z; $n = 11$ for m.uPAR-m.28z). **h**, Hemoglobin levels 20 d after cell infusion ($n = 11$ for UT; $n = 11$ for h.19-m.28z; $n = 10$ for m.uPAR-m.28z). **i**, Platelet numbers 20 d after cell infusion ($n = 11$ for UT; $n = 11$ for h.19-m.28z; $n = 10$ for m.uPAR-m.28z). **j**, Lymphocyte numbers 20 d after cell infusion ($n = 11$ for UT; $n = 11$ for h.19-m.28z; $n = 10$ for m.uPAR-m.28z). **k**, Monocyte numbers 20 d after cell infusion ($n = 11$ for UT; $n = 11$ for h.19-m.28z; $n = 10$ for m.uPAR-m.28z). **l**, Neutrophil numbers 20 d after cell infusion ($n = 11$ for UT; $n = 10$ for h.19-m.28z; $n = 10$ for m.uPAR-m.28z). **m**, Eosinophil numbers 20 d after cell infusion ($n = 11$ for UT; $n = 11$ for h.19-m.28z; $n = 10$ for m.uPAR-m.28z). Results are from two independent experiments. Data are the mean ± s.e.m.; *P* values from two-tailed unpaired Student's *t*-test (**b**–**m**).

(HFD)[31] and, indeed, obesity has been described to accelerate the 'aging clock'[32]. As in aged animals, such treatment leads to the accumulation of senescent cells[25] (Extended Data Fig. 8a–d). To test the therapeutic potential of uPAR CAR T cells in this context, we modeled metabolic syndrome by feeding mice an HFD, which induces obesity and metabolic stress[33]. After 2 months on an HFD, mice were treated with 0.5×10^6 m.uPAR-m.28z CAR T or UT cells and continued on the diet (Fig. 7a). At 20 d after infusion, mice treated with uPAR CAR T cells displayed significantly lower body weight, better fasting blood glucose levels and improvements in both glucose and insulin tolerance compared to controls (Fig. 7b–g). This therapeutic effect persisted through the period of monitoring (2.5 m after cell infusion) and was accompanied by decreased senescent cell burden in pancreas, liver and adipose tissue as assessed by SA-β-gal (Fig. 7h,i and Extended Data Fig. 8e–h). Thus, uPAR CAR T cell therapy produced a similar improvement to metabolic dysfunction in the context of metabolic syndrome in young animals as was observed in naturally aged mice.

https://doi.org/10.1038/s43587-023-00560-5

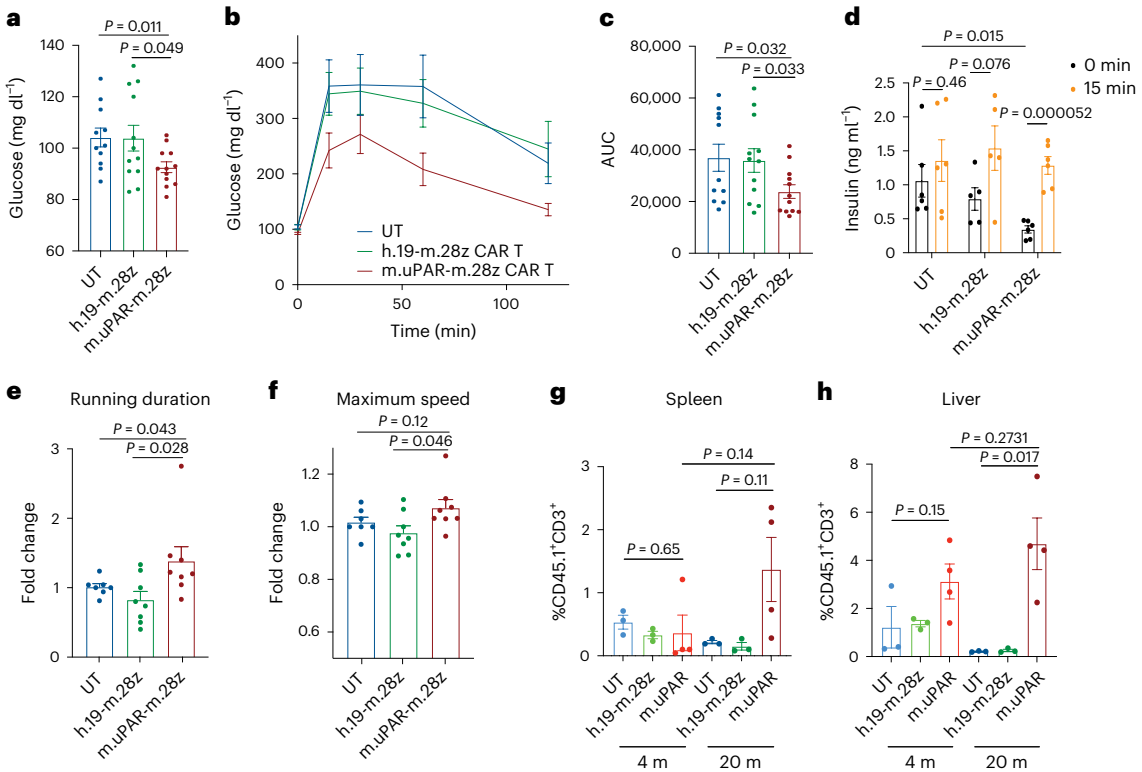

Fig. 5 | uPAR CAR T cells revert natural age-associated phenotypes. Mice were treated with m.uPAR-m.28z CAR T cells, h.19-m.28z CAR T cells or UT cells as schematized in Fig. 3a. **a**, Levels of basal glucose (mg ml^{-1}) after starvation 2.5 months after cell infusion ($n = 11$ mice for UT; $n = 12$ for h.19-m.28z and for m.uPAR-m.28z). **b**, Levels of glucose before (0 min) and after intraperitoneal administration of glucose (2 g per kg body weight) 2.5 months after cell infusion (samples sizes as in **a**). **c**, Area under the curve (AUC) representing the results from **b**. Each point represents a single mouse. **d**, Levels of insulin before and 15 min after intraperitoneal glucose administration (2 g per kg body weight) 2.5 months after cell infusion ($n = 6$ for UT; $n = 5$ for h.19-m.28z; $n = 6$ for m.uPAR-m.28z). **e**, Fold change in time to exhaustion in exercise capacity testing before cell infusion and 2.5 months after it ($n = 7$ for UT; $n = 8$ for h.19-m.28z and $n = 8$ for m.uPAR-m.28z). **f**, Fold change in maximum speed in capacity testing before cell infusion and 2.5 months after it (sample sizes as in e). **g**,**h**, Percentage of CD45.1$^+$ T cells in the spleen (**g**) or liver (**h**) of 4-month-old or 20-month-old mice 20 d after cell infusion ($n = 3$ mice per age group for UT and for h.19-m.28z; $n = 4$ for m.uPAR-m.28z). The corresponding flow cytometry gating is shown in Extended Data Fig. 10. Results are from two independent experiments (**a**–**c**, **e** and **f**) or one experiment (**d**, **g** and **h**). Data are the mean ± s.e.m.; *P* values from two-tailed unpaired Student's *t*-test (**a**, **c**, **d**, **g** and **h**) or two-tailed Mann–Whitney test (**e** and **f**).

To test whether prophylactic administration of uPAR CAR T cells could impede the development of metabolic disorders in young mice given an HFD, we administered 0.5×10^6 m.uPAR-m.28z CAR T cells 1.5 months before placement on an HFD (Fig. 7j). Remarkably, m.uPAR-m.28z CAR T cells (but not treatment with UT cells) acted prophylactically to blunt the accumulation of senescent cells over time, an effect that was also associated with decreased weight gain and glucose levels 3.5 months after infusion (Extended Data Fig. 8i–l and Fig. 7k–n). At this time, m.uPAR-m.28z CAR T cells were detectable and enriched in the spleens and livers of treated mice, where they again were composed mostly of CD8$^+$ T cells with an effector phenotype (Extended Data Fig. 9). This preventive effect on metabolic dysfunction was sustained for at least 5.5 months after cell infusion despite continuous exposure to an HFD (Fig. 7o,p).

Overall, these data highlight the contribution of uPAR-positive cells to metabolic dysfunction in aged and obese mice and raise the possibility that targeting these cells through CAR T cells could have therapeutic benefit in humans.

Discussion

Our study provides proof-of-principle evidence that senolytic cell therapies can ameliorate symptoms associated with physiological aging. We previously showed that uPAR-targeting CAR T cells could safely and effectively eliminate senescent cells in the livers of young animals[14]. Here, focusing on metabolic dysfunction as one prominent age-related pathology, we show that: (i) the fraction of uPAR-positive cells increases with age; (ii) these cells significantly contribute to the senescence burden in aged tissues; (iii) uPAR-positive cells with senescence signatures consist of both immune and non-immune populations, the latter consisting of a range of cell types that are organ dependent; (iv) uPAR CAR T cells can be effective at eliminating uPAR-positive senescent cells; (v) their effect is not associated with pathology in tissues or alterations of hepatic and renal functional parameters in aged mice; and finally, (vi) the action of uPAR CAR T cells is associated with improved glucose homeostasis and metabolic fitness in both physiological aging and HFD feeding. Importantly, at doses used to produce these therapeutic benefits, we noted no overt toxicities of uPAR CAR T cells, which could persist and expand for over 15 months as mice progressed from a youthful to an aged state.

Perhaps the most striking observation of the current work was the ability of uPAR CAR T cells to act prophylactically to blunt age-induced and diet-induced metabolic decline. Unlike senolytic approaches based on small molecules, uPAR CAR T cells have long-lasting effects after the administration of a single low dose, causing a marked impairment in age-induced or HFD-induced metabolic syndrome when mice were treated during youth or administration of HFD, respectively. Our findings are consistent with those of an earlier study that explored vaccination against GPNMB on senescent cells to address age-related pathology[34],

https://doi.org/10.1038/s43587-023-00560-5

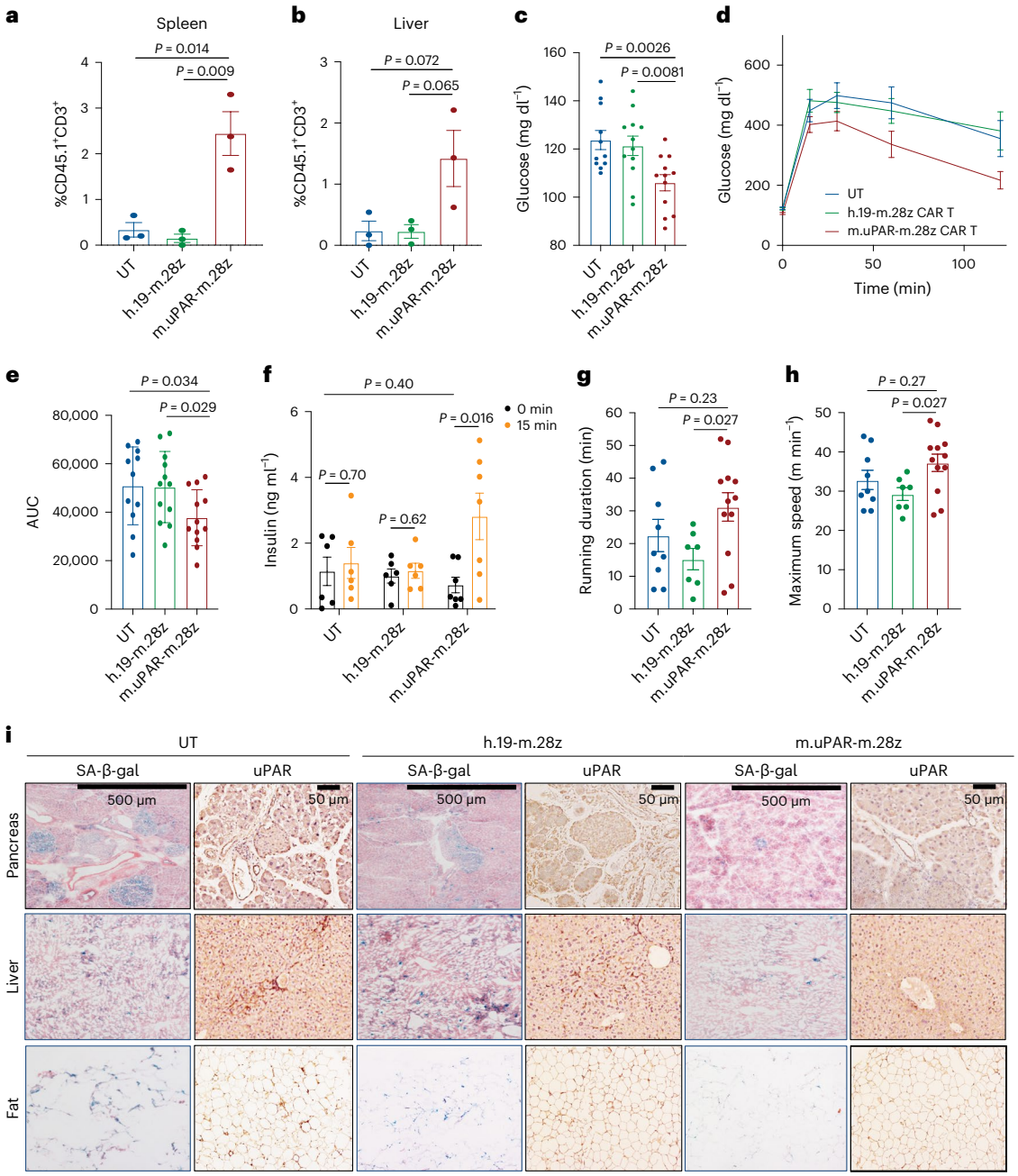

Fig. 6 | uPAR CAR T cells prevent natural age-associated phenotypes. Three- to four-month-old C57BL/6N mice were injected with 0.5×10^6 m.uPAR-m.28z CAR T cells, h.19-m.28z CAR T cells or UT cells generated from CD45.1 mice 16 h after administration of cyclophosphamide (200 mg per kg body weight). Mice were monitored over time and/or harvested at 15 months of age. **a**,**b**, Percentage of $CD45.1^+$ T cells in the spleen (**a**) or liver (**b**) of 15-month-old mice 12 months after cell infusion ($n = 3$ mice per group). **c**, Levels of basal glucose after starvation 15–18 months after cell infusion ($n = 11$ mice for UT cells; $n = 12$ for h.19-m.28z and for m.uPAR-m.28z). **d**, Levels of glucose before (0 min) and after intraperitoneal administration of glucose (2 g per kg body weight) 15–18 months after cell infusion (sample sizes as in **c**). **e**, AUC representing the results from **d**. Each point represents a single mouse. **f**, Levels of insulin (ng ml^{-1}) before and 15 min after intraperitoneal glucose (2 g per kg body weight) 15 months after cell infusion ($n = 6$ for UT cells; $n = 6$ for h.19-m.28z; $n = 7$ for m.uPAR-m.28z). **g**, Time to exhaustion in exercise capacity testing 6 months after cell infusion ($n = 9$ for UT cells; $n = 7$ for h.19-m.28z; $n = 12$ for m.uPAR-m.28z). **h**, Maximum speed (m min^{-1}) in capacity testing 6 months after cell infusion (sample sizes as in **g**). **i**, Representative staining of SA-β-gal and uPAR 15 months after cell infusion. Results are from one independent experiment (**a**, **b**, **f** and **i**) or two independent experiments (**c**–**e**, **g** and **h**). Data are the mean ± s.e.m.; *P* values from two-tailed unpaired Student's *t*-test (**a**–**c**, **e** and **f**) or two-tailed Mann–Whitney test (**g** and **h**).

although with our cellular therapy, both effect sizes and duration were substantially larger. In fact, our results demonstrate a protective effect for over a year in the context of physiological aging in the laboratory mouse, a species with an average lifespan of around 2 years.

Studies using genetic or pharmacological approaches to senolysis have been equivocal as to whether elimination of senescent cells will significantly extend longevity[29,30,35]. Our current studies are not sufficiently powered to draw conclusions on longevity at this stage. As senescent cells contribute to a range of age-related tissue pathologies, studying the impact of senolysis in aged animals provides an opportunity to interrogate multiple comorbidities under similar conditions. Future studies will evaluate the potential of uPAR CAR T cells (or other

https://doi.org/10.1038/s43587-023-00560-5

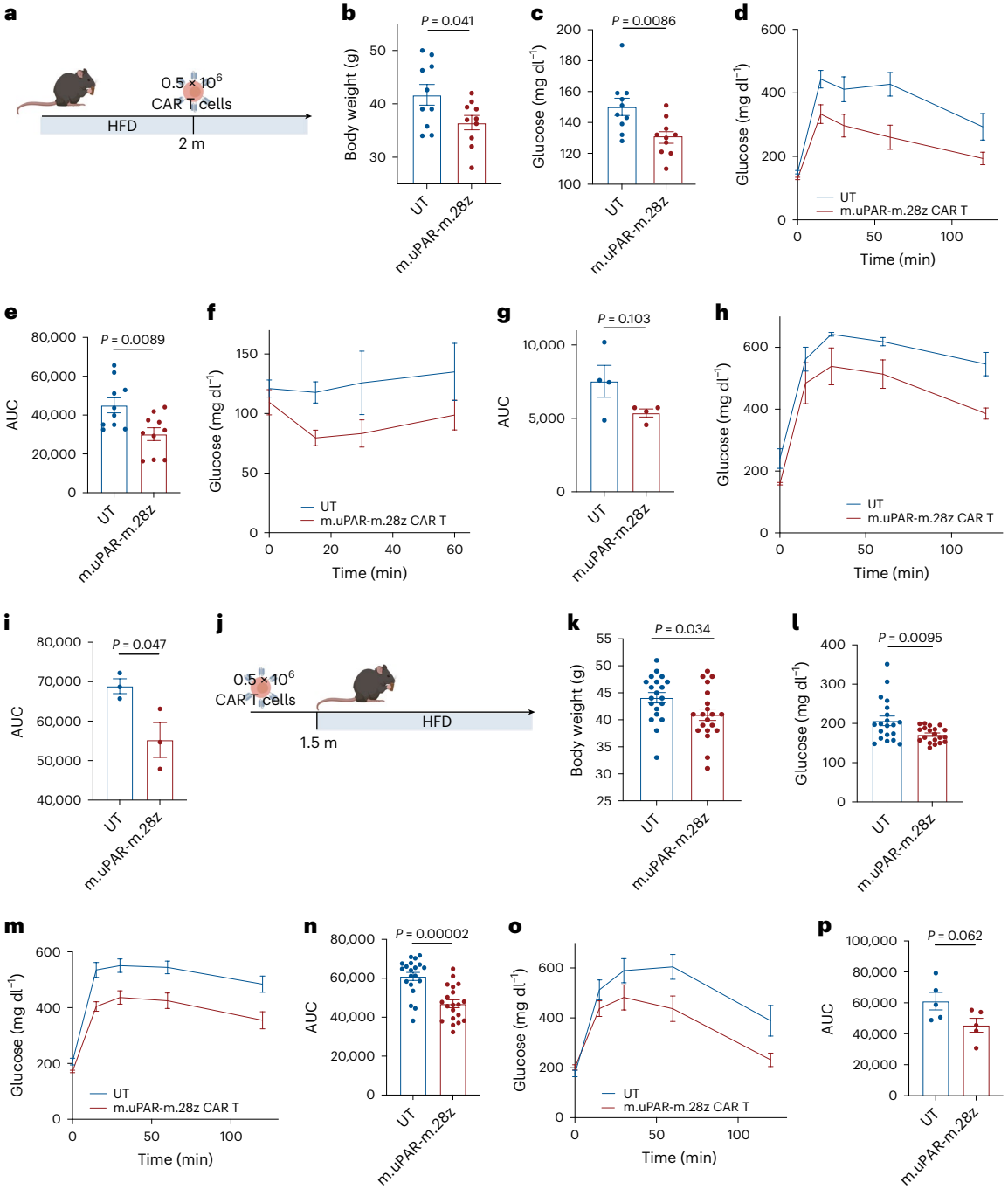

Fig. 7 | uPAR CAR T cells are therapeutic and preventive in metabolic syndrome. a, Experimental scheme for **b**–**i**. Three-month-old C57BL/6N mice were treated with an HFD for 2 months followed by intravenous infusion with 0.5×10^6 m.uPAR-m.28z or UT cells 16 h after administration of cyclophosphamide (200 mg per kg body weight). Mice were euthanized 1 month later or monitored over time. **b**, Body weight 1 month after cell infusion ($n = 10$ mice per group). **c**, Basal glucose levels after starvation at 1 month after cell infusion ($n = 10$ mice per group). **d**, Glucose levels before (0 min) and after intraperitoneal administration of glucose (1 g per kg body weight) 1 month after cell infusion ($n = 10$ mice per group). **e**, AUC representing the results from **d**. **f**, Glucose levels before (0 min) and after intraperitoneal administration of insulin (0.5 units per kg body weight) 1 month after cell infusion ($n = 4$ mice per group). **g**, AUC representing the results from **f**. Each point represents a single mouse. **h**, Glucose levels before (0 min) and after intraperitoneal glucose administration (1 g per kg body weight) 2.5 months after cell infusion ($n = 3$ mice per group). **i**, AUC representing the results from **h**. Each point represents a single mouse. **j**, Experimental scheme for **k**–**p**. Three-month-old C57BL/6N mice were intravenously infused with 0.5×10^6 m.uPAR-m.28z or UT cells 16 h after administration of cyclophosphamide (200 mg per kg body weight). At 1.5 months after infusion, mice were placed on an HFD, then euthanized 2 months later or monitored over time. **k**, Body weight at 3.5 months after cell infusion ($n = 20$ mice per group). **l**, Basal glucose levels after starvation 3.5 months after cell infusion ($n = 20$ mice per group). **m**, Levels of glucose before (0 min) and after intraperitoneal administration of glucose (1 g per kg body weight) 1 month after cell infusion ($n = 20$ mice per group). **n**, AUC representing the results from **m**. **o**, Glucose levels before (0 min) and after intraperitoneal glucose administration (1 g per kg body weight) 5.5 months after cell infusion ($n = 5$ mice per group). **p**, AUC representing the results from **o**. Each point represents a single mouse (**a**–**p**). Results are from two independent experiments (**b**–**e** and **k**–**n**) or one independent experiment (**f**–**i**, **o** and **p**). Data are the mean ± s.e.m.; *P* values derived from two-tailed unpaired Student's *t*-test (**b**, **c**, **e**, **g**, **i**, **k**, **l**, **n** and **p**). Schematics were created with BioRender.com.

senolytic cell therapies) in additional aging and related tissue-damage pathologies, the latter disease contexts providing a more likely starting point for clinical implementation.

It remains to be determined which of the uPAR-positive cell populations targeted by uPAR CAR T cells are responsible for the improved metabolic function we observe. In other senolytic studies, the elimination of senescent pancreatic beta cells has been linked to improved glucose tolerance[25]. However, there are reports suggesting that targeting senescent cells in adipose tissue[28] or even immune cell senescence[36] may also play a role. In this regard, recent studies suggest that the elimination of macrophage populations with senescent features can also improve tissue decline in mice[37,38]. Whether or not these macrophages are truly 'senescent' or have an alternative cell state is a topic of debate; regardless, given that we observe a fraction of uPAR-expressing macrophages that also coexpress SA-β-gal and senescence-associated transcriptional signatures accumulating in aged tissues, it seems likely that their elimination contributes to the phenotypes we observe.

While the mechanism of action of most current small molecules is often inferred or poorly understood, senolytic CAR T cells have a clear underlying rationale based on the expression of a specific surface antigen. While toxicity issues are invariably a concern, cellular therapy harbors the versatility to simultaneously target several surface antigens through AND gate approaches[11], modulate persistence through different CAR designs[39] and/or incorporate safety switches[40], all of which provide avenues to mitigate side effects that are not possible through vaccination strategies or small-molecule approaches[40]. Indeed, another recent report reveals that mice and primates tolerate CAR T cells that target a natural killer cell ligand that is upregulated on senescent cells and other cell types[41]. Taken together, these efforts could result in the identification of tissue-specific senolytic antigens that could be targeted with cellular therapy to treat different age-related phenotypes. The persistence of the uPAR-targeted CAR T cells and the durability of the effects after a single low-dose treatment highlight the clinical potential of the senolytic CAR T cell approach for the treatment of chronic pathologies.

Methods

Mice

All mouse experiments were approved by the MSKCC and/or CSHL Internal Animal Care and Use Committee (animal protocol 11-06-011 at MSKCC and 21-4 at CSHL). All relevant animal use guidelines and ethical regulations were followed. Mice were maintained under specific pathogen-free conditions. Housing was on a 12-h–12-h light–dark cycle under standard temperature and humidity of approximately 18–24 °C and 40–60%, respectively. The following mice were used: 3- to 4-month-old C57BL/6 mice (purchased from Charles River), 18-month-old C57BL/6 mice (obtained from the National Institute of Aging) and 6-week-old B6.SJL-Ptrca/BoyAiTac (CD45.1) mice (purchased from Taconic). Mice of both sexes were used at 8–12 weeks of age and 18–20 months of age for the aging experiments, males of 8–12 weeks old for the HFD experiments and females of 6–10 weeks old for T cell isolation. Mice were kept in group housing. Mice had free access to food and water except during the starvation period before glucose or insulin tolerance testing. Aging mice were fed a normal diet (PicoLab Rodent Diet 20, LabDiet), mice on the HFD experiments were fed an HFD (TD.06414, 60% of kcal from fat; Envigo).

Flow cytometry

For in vivo sample preparation, livers were dissociated using the MACS liver dissociation kit (Miltenyi Biotec, 130-1-5-807), filtered through a 100-µm strainer and washed with PBS, and red blood cells were lysed by an ammonium–chloride–potassium (ACK) lysing buffer (Lonza). Cells were washed with PBS, resuspended in FACS buffer and either used for immediate analysis or fixed with Fixation Buffer (BD Biosciences, 554655) according to the manufacturer's instructions and used for later analysis. Spleens were mechanically disrupted with the back of a 5-ml syringe, filtered through a 40-µm strainer and washed with PBS and 2 mM EDTA; then red blood cells were lysed by ACK lysing buffer (Lonza). Gonadal adipose tissue was dissociated as described[42]. In short, adipose tissue was isolated and placed in a digestion solution consisting of 4 mg ml^{-1} collagenase, type II (Sigma) in DPBS (Life Technologies) supplemented with 0.5% BSA (Sigma) and 10 mM $CaCl_2$ digested at 37 °C for 20 min in a rotational shaker. Afterwards, samples were mechanically dissociated with a 10-ml serological pipette, filtered through a 40-µm strainer and washed with PBS and 2 mM EDTA; then red blood cells were lysed by ACK lysing buffer (Lonza). Pancreata were placed into cold DMEM with 10% FBS and penicillin and streptomycin. The pancreata were minced in this media on ice into 2- to 4-mm fragments so that they would pass through the end of a 1-ml pipette tip with ease. The minced tissue was collected in a 15-ml Falcon tube and dissociated in 100 mg ml^{-1} Dispase (Life Technologies, 17105041), 20 mg ml^{-1} collagenase P (Roche, 11249002001) and 1 mM EDTA for 20 min on a heated rocker at 37 °C (Eppendorf). After 20 min, 5 ml of DMEM with 10% FBS was added to quench the reaction. The supernatant was removed and filtered through a 100-µm filter (VWR). Next, 5 ml of dissociation media consisting of 100 mg ml^{-1} Dispase (Life Technologies, 17105041), 20 mg ml^{-1} collagenase P (Roche, 11249002001) and 1 mM EDTA was added before replacing the 15-ml tube into the heated rocker for 20 min. The reaction was quenched again after 20 min with media and filtered via a 100-µm filter. The dissociated cells were spun at 500 r.c.f. for 10 min in a swinging-bucket centrifuge. The supernatant was discarded, and the cells were resuspended in ACK lysis buffer for 2–4 min in ice. Cells were washed with PBS, resuspended in FACS buffer and either used for immediate analysis or fixed with Fixation Buffer (BD Biosciences, 554655) and used for later analysis.

Fc receptors were blocked using FcR blocking reagent, mouse (Miltenyi Biotec). The following fluorophore-conjugated antibodies were used in the indicated dilutions: Myc-tag AF647 (clone 9B11, Cell Signaling Technology, 2233S, 25; 1:50 dilution), m.CD45.1 BV785 (clone A20, BioLegend, 110743, B347719; 1:100 dilution), m.CD45.2 BV785 (clone 104, BioLegend, 109839, B343292; 1:100 dilution), mCD3 AF488 (clone 17A2, BioLegend, 100210, B284975; 1:100 dilution), mCD4 BUV395 (clone GK1.5, BD, 563790, 1097734; 1:50 dilution), mCD8 PE-Cy7 (clone 53-6.7, BioLegend, 100722, B312604; 1:50 dilution), mCD62L BV421 (clone MEL-14, BioLegend, 104435, B283191; 1:50 dilution), mCD44 APC-Cy7 (clone IM7, BD Pharminogen, 560568, 1083068; 1:100 dilution), mCD3 BV650 (clone 17A2, BioLegend, 100229, B350667; 1:100 dilution), mCD19 BV650 (clone 1D3, BD Biosciences, 563235, 1354015; 1:100 dilution), mNKp46 BV650 (clone 29A1.4, BioLegend, 137635, B298809; 1:100 dilution), mCD11b BUV395 (clone M1/70, BD Biosciences, 563553, 0030272; 1:50 dilution), mLy-6C APC-Cy7 (clone HK1.4, BioLegend, 128026, B375238; 1:100 dilution), mly6G BV605 (clone 1A8, BD Biosciences, 563005, 2144780; 1:100 dilution), m.uPAR AF700 (R&D systems, FAB531N, 1656339; 1:50 dilution), m.uPAR PE (R&D systems, FAB531P, ABLH0722051; 1:50 dilution), mF4/80 PE-eFluor610 (clone BM8, Invitrogen, 61-4801-82, 2338698; 1:100 dilution), 7-AAD (BD, 559925, 9031655; 1:40 dilution) or Ghost UV 450 Viability Dye (13-0868-T100, Tonbo Biosciences, D0868083018133, 1 µl ml^{-1}) was used as viability dye. Flow cytometry was performed on an LSRFortessa instrument (BD Biosciences), FACS was performed on a SONY SH800S cell sorter and data were analyzed using FlowJo (TreeStar).

Single-cell RNA-seq

Sequencing data was demultiplexed, mapped, and processed into gene/cell expression matrices using 10x Genomics' Cell Ranger software v7.1.0 (https://support.10xgenomics.com/single-cell-gene-expression/software/pipelines/latest/what-is-cell-ranger/).

Gene expression reads were aligned to the mouse reference genome version gex-mm10-2020-A, available from the 10x Genomics website. We kept cells using the following parameters: 'min.cells > 10, nFeature_RNA > 500, nCount_RNA > 2,500, percent.mt < 15'. Gene expression count data were normalized using SCTransform to regress out the percentage of mitochondrial RNA. The R package BBKNN was used to remove batch effects between mouse samples, and 0.5 was used as expression cutoff to define uPAR High cell populations. Clusters were identified using a resolution of 0.8, and cell types were annotated using R packages celldex, SingleR, Azimuth and custom gene sets[20,21]. Known markers for each cell type were plotted using the DotPlot function in Seurat. Senescence gene sets from refs. 17,24 were used to calculate signature scores using the AddModuleScore function in Seurat, and a signature score cutoff of 0.05 was used to define Senescence High cell populations. Differential expression analysis and functional annotations of gene sets were analyzed in the following way: Differential gene expression analysis was performed by comparing all the uPAR-positive versus uPAR-negative cells using RunPresto in Seurat, and the differentially expressed genes (DEGs) were determined by >1.5-fold change in gene expression with adjusted P value < 0.1. Pathway enrichment analysis was performed using the msigDB Hallmark gene sets using enrichR[43]. Significance of the tests was assessed using combined score, described as $c = \log(P) \times z$, where c is the combined score, P is Fisher's exact test P value, z is the z-score for deviation from expected rank, and adjusted P values defined by enrichR. A lollipop plot was generated by plotting the top enriched/depleted $\log_2$(combined.score) on the x axis (directional), and size and color of the dots represents by $-\log_{10}$(adjusted P value).

Isolation, expansion and transduction of mouse T cells

B6.SJL-Ptrca/BoyAiTac mice (CD45.1 mice) were euthanized and spleens were collected. After tissue dissection and red blood cell lysis, primary mouse T cells were purified using the mouse Pan T cell Isolation Kit (Miltenyi Biotec). Purified T cells were cultured in RPMI-1640 (Invitrogen) supplemented with 10% FBS (HyClone), 10 mM HEPES (Invitrogen), 2 mM L-glutamine (Invitrogen), MEM non-essential amino acids 1× (Invitrogen), 55 µM β-mercaptoethanol, 1 mM sodium pyruvate (Invitrogen), 100 IU ml^{-1} recombinant human IL-2 (Proleukin; Novartis) and mouse anti-CD3/28 Dynabeads (Gibco) at a bead:cell ratio of 1:2. T cells were spinoculated with retroviral supernatant collected from Phoenix-ECO cells 24 h after initial T cell activation as described in refs. 44,45 and used for functional analysis 3–4 d later.

Genetic modification of T cells

The mouse SFG γ-retroviral m.uPAR-m28z plasmid has been described[14]. The mouse SFG γ-retroviral h.19-m28z plasmid[14] was constructed by stepwise Gibson assembly (New England BioLabs) using the amino acid sequence for the scFv specific for human CD19 of the SFG-1928z backbone[46] and cloned into the backbone of the SFG γ-retroviral m.uPAR-m28z plasmid[14]. In both constructs, the anti-mouse uPAR scFv or anti-human CD19 scFv is preceded by a mouse CD8A leader peptide and followed by the Myc-tag sequence (EQKLISEEDL), mouse CD28 transmembrane and intracellular domain and mouse CD3z intracellular domain[44,45]. Plasmids encoding the SFGγ retroviral vectors were used to transfect gpg29 fibroblasts (H29) to generate VSV-G pseudotyped retroviral supernatants, which were used to construct stable retrovirus-producing cell lines as described[44,46].

Glucose tolerance testing

Blood samples from mice fasted for 8–12 h were collected at 0, 15, 30, 60 and 120 min after intraperitoneal injections of glucose (Sigma-Aldrich; 2 g per kg body weight for aging experiments and 1 g per kg body weight for HFD experiments). Insulin was measured from serum collected at the 0-min and 15-min time points. Concentrations were determined using the UltraSensitive Mouse Insulin ELISA kit (Crystal Chem, 90080).

Insulin tolerance testing

Blood samples from mice fasted for 4 h were collected at 0, 15, 30 and 60 min after intraperitoneal injections of insulin (Humulin R; Eli Lilly; 0.5 units per kg body weight).

Histological analysis

Tissues were fixed overnight in 10% formalin, embedded in paraffin and cut into 5-µm sections. Sections were subjected to H&E staining. Immunohistochemical staining was performed following standard protocols. The following antibodies were used: anti-mouse uPAR (AF534, R&D, DCL0521042; 1:50 dilution) and horse anti-goat IgG (30116; Vector Laboratories, ZH0526). Three fields per section were counted per sample with Fiji-ImageJ and averaged to quantify the percentage of uPAR-positive area per field. SA-β-gal staining was performed as previously described[47] at a pH of 5.5 for mouse tissues. Specifically, fresh frozen tissue sections were fixed with 0.5% glutaraldehyde in PBS for 15 min, washed with PBS supplemented with 1 mM $MgCl_2$ and stained for 5–8 h in PBS containing 1 mM $MgCl_2$, 1 mg ml^{-1} X-gal, 5 mM potassium ferricyanide and 5 mM potassium ferrocyanide. Tissue sections were counterstained with eosin. Three fields per section were counted with ImageJ and averaged to quantify the percentage of SA-β-gal-positive area per field.

Immunofluorescence analysis

For the fluorescent SA-β-gal labeling, tissue slides were exposed to the C12RG substrate at 37 °C according to manufacturer's instructions (ImaGene Red C12RG lacZ Gene Expression Kit, Molecular Probes, I2906)[48,49]. Subsequently, for immunofluorescence analysis, slides were fixed with 4% paraformaldehyde for 10 min at room temperature and regular immunofluorescence was performed following standard protocols and those previously described[14]. The following antibodies were used: anti-mouse uPAR uPAR (AF534,R&D, DCL0521042; 1:50 dilution) and anti-mouse F4/80 (Bio-Rad, CI:A3-1, 155529; 1:100 dilution). For quantification, five high-power fields per section were counted and averaged to quantify the percentage of SA-β-gal^+, $uPAR^+$ and $F4/80^+$ per DAPI-positive cells. For colocalization analysis, Pearson coefficient was calculated using ImageJ.

Exercise capacity testing

Exercise capacity was assessed using a motorized treadmill (model 1050 EXER 3/6; Columbus Instruments). For 3 d before testing, mice were acclimatized to the treadmill (the mice walked on the treadmill at 10 m min^{-1} for 10 to 15 min per day). Following acclimatization, all mice underwent exercise capacity tests on consecutive days. Tests began with mice walking at 10 m min^{-1} with speed increased by 2 m min^{-1} every 2 min until exhaustion (mice could no longer achieve treadmill running speed despite repeated encouragement). The primary end points were time to exhaustion and maximum speed.

Blood measurements

Complete blood counts with differentials were performed using an automated hematology analyzer (IDEXX Procyte DX). For serum chemistry, blood was collected in tubes containing a serum separator. The tubes were then centrifuged, and the serum was obtained for analysis. Serum chemistry was performed by the LCP on a Beckman Coulter AU680 analyzer (Beckman Coulter Life Sciences). For cytokine analysis, plasma was collected and samples were processed and measured by Eve Technologies.

Pathology

Mice submitted for postmortem examination were euthanized by CO_2 asphyxiation and cardiac exsanguination. Complete necropsies were performed at the Laboratory of Comparative Pathology (MSK, the Rockefeller University, and Weill Cornell Medicine). Representative sections were taken from all organ systems including heart, thymus, lungs,

esophagus, trachea, thyroid glands, spleen, pancreas, liver, gallbladder, kidneys, adrenal glands, stomach, duodenum, jejunum, ileum, cecum, colon, lymph nodes (mesenteric and submandibular), salivary glands, skin (trunk and head), urinary bladder, epididymides, testes, prostate, seminal vesicles, uterus, cervix, vagina, ovaries, oviducts, spinal cord, vertebrae, sternum, femur, tibia, stifle joint, skeletal muscle, nerves, skull, nasal cavity, oral cavity, teeth, ears, eyes, pituitary gland and brain. Sections were fixed in 10% neutral-buffered formalin, processed in alcohol and xylene, embedded in paraffin, sectioned (5 µm thick) and stained with H&E. The skull, spinal column, sternum and hindlimb were decalcified in a formic acid and formaldehyde solution (Surgipath Decalcifier I, Leica Biosystems) before processing. H&E-stained tissue sections were evaluated by a board-certified veterinary pathologist (S.E.C.). Representative images were captured using a brightfield BX45 microscope with a DP26 camera and cellSens (version 1.18) Dimension software (Olympus America).

Statistical analysis

Data are presented as the mean ± s.e.m. Statistical analysis was performed by Student's *t*-test or Mann–Whitney test using Prism v9.3.1 (GraphPad software). No statistical methods were used to predetermine sample size in the mouse studies, and no randomization method was used to allocate mice to experimental groups. Mouse conditions were observed by an operator who was blinded to the treatment groups in addition to the main investigator who was not blind to group allocation. Pathological analysis and exercise testing studies were performed in a blinded fashion. Data analysis was not performed in a blinded fashion. Data analysis was based on objectively measurable data (cell count, blood tests). No data were excluded except for histological assessment of HFD experiments, where we excluded OCT cassettes of samples containing adipose tissue or pancreas that were folded and presented a morphology that did not allow for successful slide generation; these were not further processed. Data distribution was assumed to be normal, but this was not formally tested. No adjustment for multiple comparisons was performed. The rationale for this was that to increase the rigor of select analyses, two control groups were compared to the experimental group, but it could have been biologically possible to just have one control group. Thus, for any given endpoint, there were two pairwise comparisons: the experiment group separately compared to each control. While two tests were evaluated, we only considered the analysis statistically significant if both tests had a P value less than 0.05. If only one of the two tests was significant, we did not claim the groups were significantly different; instead, we considered the analysis inconclusive and reported a trend. Viewing the analysis as significant only if both P values were less than 0.05 preserves the family-wise error rate at less than 0.05. Figures were prepared using BioRender.com for scientific illustrations in Figs. 3a and 7a,j, GraphPad Prism v9.3.1, and Microsoft Excel v16.77 and Illustrator CC 2022 (Adobe).

Reporting summary

Further information on research design is available in the Nature Portfolio Reporting Summary linked to this article.

Data availability

scRNA-seq data are deposited in the Gene Expression Omnibus under accession number GSE243616. Data from the Tabula Muris Senis project[18] were accessed through https://twc-stanford.shinyapps.io/maca/. Human data from ref. 26 were accessed through https://zenodo.org/records/7311202#.Y20ybezMIyl/. Source data are provided with this paper. Requests for materials should be addressed to C.A.

Code availability

All code is available at https://github.com/naikai/Amor_et_al_2023/.

References

1. Sharpless, N. E. & Sherr, C. J. Forging a signature of in vivo senescence. *Nat. Rev. Cancer* **15**, 397–408 (2015).
2. Collado, M., Blasco, M. A. & Serrano, M. Cellular senescence in cancer and aging. *Cell* **130**, 223–233 (2007).
3. Coppe, J. P. et al. Senescence-associated secretory phenotypes reveal cell-nonautonomous functions of oncogenic RAS and the p53 tumor suppressor. *PLoS Biol.* **6**, 2853–2868 (2008).
4. Ovadya, Y. et al. Impaired immune surveillance accelerates accumulation of senescent cells and aging. *Nat. Commun.* **9**, 5435 (2018).
5. Lopez-Otin, C., Blasco, M. A., Partridge, L., Serrano, M. & Kroemer, G. The hallmarks of aging. *Cell* **153**, 1194–1217 (2013).
6. Munoz-Espin, D. et al. A versatile drug delivery system targeting senescent cells. *EMBO Mol. Med.* **10**, e9355 (2018).
7. Childs, B. G. et al. Senescent intimal foam cells are deleterious at all stages of atherosclerosis. *Science* **354**, 472–477 (2016).
8. Bussian, T. J. et al. Clearance of senescent glial cells prevents tau-dependent pathology and cognitive decline. *Nature* **562**, 578–582 (2018).
9. Childs, B. G., Durik, M., Baker, D. J. & van Deursen, J. M. Cellular senescence in aging and age-related disease: from mechanisms to therapy. *Nat. Med.* **21**, 1424–1435 (2015).
10. Zhang, L., Pitcher, L. E., Prahalad, V., Niedernhofer, L. J. & Robbins, P. D. Targeting cellular senescence with senotherapeutics: senolytics and senomorphics. *FEBS J.* **290**, 1362–1383 (2023).
11. Sadelain, M., Riviere, I. & Riddell, S. Therapeutic T cell engineering. *Nature* **545**, 423–431 (2017).
12. Melenhorst, J. J. et al. Decade-long leukaemia remissions with persistence of $CD4^+$ CAR T cells. *Nature* **602**, 503–509 (2022).
13. Smith, H. W. & Marshall, C. J. Regulation of cell signalling by uPAR. *Nat. Rev. Mol. Cell Biol.* **11**, 23–36 (2010).
14. Amor, C. et al. Senolytic CAR T cells reverse senescence-associated pathologies. *Nature* **583**, 127–132 (2020).
15. Rasmussen, L. J. H. et al. Association between elevated suPAR, a new biomarker of inflammation, and accelerated aging. *J. Gerontol. A Biol. Sci. Med. Sci.* **76**, 318–327 (2021).
16. Tanaka, T. et al. Plasma proteomic biomarker signature of age predicts health and life span. *eLife* **9**, e61073 (2020).
17. Saul, D. et al. A new gene set identifies senescent cells and predicts senescence-associated pathways across tissues. *Nat. Commun.* **13**, 4827 (2022).
18. The Tabula Muris Consortium. A single-cell transcriptomic atlas characterizes ageing tissues in the mouse. *Nature* **583**, 590–595 (2020).
19. Liu, Y., Beyer, A. & Aebersold, R. On the dependency of cellular protein levels on mRNA abundance. *Cell* **165**, 535–550 (2016).
20. Aran, D. et al. Reference-based analysis of lung single-cell sequencing reveals a transitional profibrotic macrophage. *Nat. Immunol.* **20**, 163–172 (2019).
21. Hao, Y. et al. Integrated analysis of multimodal single-cell data. *Cell* **184**, 3573–3587 (2021).
22. Mederacke, I., Dapito, D. H., Affo, S., Uchinami, H. & Schwabe, R. F. High-yield and high-purity isolation of hepatic stellate cells from normal and fibrotic mouse livers. *Nat. Protoc.* **10**, 305–315 (2015).
23. Lee, H. & Engin, F. Preparing highly viable single-cell suspensions from mouse pancreatic islets for single-cell RNA sequencing. *STAR Protoc.* **1**, 100144 (2020).
24. Tasdemir, N. et al. BRD4 connects enhancer remodeling to senescence immune surveillance. *Cancer Discov.* **6**, 612–629 (2016).
25. Aguayo-Mazzucato, C. et al. Acceleration of beta cell aging determines diabetes and senolysis improves disease outcomes. *Cell Metab.* **30**, 129–142 (2019).

26. Shrestha, S. et al. Aging compromises human islet beta cell function and identity by decreasing transcription factor activity and inducing ER stress. *Sci. Adv.* **8**, eabo3932 (2022).
27. Ferrucci, L. & Fabbri, E. Inflammageing: chronic inflammation in ageing, cardiovascular disease, and frailty. *Nat. Rev. Cardiol.* **15**, 505–522 (2018).
28. Xu, M. et al. Targeting senescent cells enhances adipogenesis and metabolic function in old age. *eLife* **4**, e12997 (2015).
29. Xu, M. et al. Senolytics improve physical function and increase lifespan in old age. *Nat. Med.* **24**, 1246–1256 (2018).
30. Baker, D. J. et al. Naturally occurring p16(Ink4a)-positive cells shorten healthy lifespan. *Nature* **530**, 184–189 (2016).
31. Buettner, R., Scholmerich, J. & Bollheimer, L. C. High-fat diets: modeling the metabolic disorders of human obesity in rodents. *Obesity* **15**, 798–808 (2007).
32. Etzel, L. et al. Obesity and accelerated epigenetic aging in a high-risk cohort of children. *Sci. Rep.* **12**, 8328 (2022).
33. Liu, Z. et al. High-fat diet induces hepatic insulin resistance and impairment of synaptic plasticity. *PLoS ONE* **10**, e0128274 (2015).
34. Suda, M. et al. Senolytic vaccination improves normal and pathological age-related phenotypes and increases lifespan in progeroid mice. *Nat. Aging* **1**, 1117–1126 (2021).
35. Baker, D. J. et al. Clearance of p16Ink4a-positive senescent cells delays ageing-associated disorders. *Nature* **479**, 232–236 (2011).
36. Yi, H. S. et al. T-cell senescence contributes to abnormal glucose homeostasis in humans and mice. *Cell Death Dis.* **10**, 249 (2019).
37. Prieto, L. I. et al. Senescent alveolar macrophages promote early-stage lung tumorigenesis. *Cancer Cell* **41**, 1261–1275 (2023).
38. Haston, S. et al. Clearance of senescent macrophages ameliorates tumorigenesis in KRAS-driven lung cancer. *Cancer Cell* **41**, 1242–1260 (2023).
39. Feucht, J. et al. Calibration of CAR activation potential directs alternative T cell fates and therapeutic potency. *Nat. Med.* **25**, 82–88 (2019).
40. Gargett, T. & Brown, M. P. The inducible caspase-9 suicide gene system as a 'safety switch' to limit on-target, off-tumor toxicities of chimeric antigen receptor T cells. *Front. Pharmacol.* **5**, 235 (2014).
41. Yang, D. et al. NKG2D-CAR T cells eliminate senescent cells in aged mice and nonhuman primates. *Sci. Transl. Med.* **15**, eadd1951 (2023).
42. Orr, J. S., Kennedy, A. J. & Hasty, A. H. Isolation of adipose tissue immune cells. *J. Vis. Exp.* **75**, e50707 (2013).
43. Chen, E. Y. et al. Enrichr: interactive and collaborative HTML5 gene list enrichment analysis tool. *BMC Bioinformatics* **14**, 128 (2013).
44. Kuhn, N. F. et al. CD40 ligand-modified chimeric antigen receptor T cells enhance antitumor function by eliciting an endogenous antitumor response. *Cancer Cell* **35**, 473–488 (2019).
45. Davila, M. L., Kloss, C. C., Gunset, G. & Sadelain, M. CD19 CAR-targeted T cells induce long-term remission and B Cell Aplasia in an immunocompetent mouse model of B cell acute lymphoblastic leukemia. *PLoS ONE* **8**, e61338 (2013).
46. Brentjens, R. J. et al. Eradication of systemic B-cell tumors by genetically targeted human T lymphocytes co-stimulated by CD80 and interleukin-15. *Nat. Med.* **9**, 279–286 (2003).
47. Ruscetti, M. et al. NK cell-mediated cytotoxicity contributes to tumor control by a cytostatic drug combination. *Science* **362**, 1416–1422 (2018).
48. Debacq-Chainiaux, F., Erusalimsky, J. D., Campisi, J. & Toussaint, O. Protocols to detect senescence-associated beta-galactosidase (SA-β-gal) activity, a biomarker of senescent cells in culture and in vivo. *Nat. Protoc.* **4**, 1798–1806 (2009).
49. Cahu, J. & Sola, B. A sensitive method to quantify senescent cancer cells. *J. Vis. Exp.* **78**, e50494 (2013).
50. Snyder, J. M. et al. Validation of a geropathology grading system for aging mouse studies. *Geroscience* **41**, 455–465 (2019).
51. McInness, E. *Background Lesions in Laboratory Animals* (Elsevier, 2012).

Acknowledgements

We thank C. J. Sherr and J. Novak for insightful discussions. We thank the members of the animal facilities at Cold Spring Harbor Laboratory and Memorial Sloan Kettering Cancer Center, without whom this work would not have been possible. We thank J. Habel, R. Rubino, L. Bianco, E. Earl, M. Labarbera, J. Coblentz and A. Bjertnes for outstanding animal care. We thank C. Regan and J. Preall for technical support in performing scRNA-seq. We thank E. de Stanchina, K. Chen, G. Gunset, P. Moody, L. Tellez Perez, M. Trousdell and D. Chatterjee for technical assistance. We thank S. Devlin and T. Ha for statistical consultation and assistance. I.F.-M. was supported by a postgraduate fellowship from La Caixa foundation and a Momentum fellowship from the Mark Foundation for Cancer Research. J.F. was supported by the Starting Grant of the European Research Council, ERC-StG-949667. V.J.A.B. was supported by a Francois Wallace Monahan Fellowship from the JLM Benevolent Fund and a Cancer Research Institute Irvington fellowship. R.M. was supported by a Rubicon postdoctoral fellowship from the Netherlands Organization for Scientific Research and a Cancer Research Institute Irvington fellowship. D.A.T. is supported by the Lustgarten Foundation, where he is a distinguished scholar and Director of the Lustgarten Foundation–designated Laboratory of Pancreatic Cancer Research. D.A.T. is also supported by the Thompson Foundation, the Pershing Square Foundation, the Cold Spring Harbor Laboratory and Northwell Health Affiliation, the Northwell Health Tissue Donation Program, the Cold Spring Harbor Laboratory Association, the Simons Foundation (552716) and the National Institutes of Health (5P30CA45508, U01CA210240, R01CA229699, U01CA224013, 1R01CA188134 and 1R01CA190092). R.L.L. received funding that additionally supported this work from an R35 grant from the National Institute of Cancer (CA197594) and a collaborative U01 Research Project grant from the National Institute of Aging (the U01 grant was jointly received with the laboratory of Jenniffer Trowbridge at the Jackson Laboratories (U01AG077925; 210374-0622-02). This work was performed with assistance from the US National Institutes of Health grant S10OD028632-01. This work was also supported by an R01 grant from the National Institute of Aging (AG065396 to S.W.L. and M.S.) and a Technology Development Fund project grant from MSKCC (S.W.L.) and the Cancer Center Support grants 5P30CA045508 (CSHL) and P30 CA008748 (MSKCC). M.S. also receives support from the Pasteur-Weizmann/Servier and Leopold Griffuel Awards and is the Stephen and Barbara Friedman Chair at MSKCC. S.W.L is the Geoffrey Beene Chair of Cancer Biology at MSKCC and a Howard Hughes Medical Institute Investigator. C.A. received support from the Early Independence Award (DP5; 1DP5OD033055-01) from the National Institutes of Health Common Fund, Developmental Funds from the Cancer Center Support grant P30CA045508, a Longevity Impetus Grant from the Norn Group and an R01 grant from the National Institute of Aging (1R01 AG082800-01). The funders had no role in study design, data collection and analysis, decision to publish or preparation of the manuscript.

Author contributions

C.A. conceived the project; acquired funding; designed, performed, analyzed and supervised experiments; and wrote the paper with assistance from all authors. I.F.-M. designed, performed and analyzed experiments and edited the paper. Y.-J.H. analyzed the scRNA-seq datasets. S.E.C. performed the histological assessment of toxicities. S.C., S.N., C.G., E.N.-J., J.F., C.H., V.J.A.B., J.A.B. and R.M.

designed, performed and analyzed experiments. M.G.W. provided technical support. D.A.T. reviewed the manuscript. R.L.L. reviewed the manuscript. L.W.J. designed and supervised experiments and reviewed the manuscript. M.S. acquired funding, supervised experiments and reviewed the manuscript. S.W.L. conceived the project, acquired funding, supervised experiments and edited the paper. All authors read and approved the paper.

Competing interests

C.A., J.F., M.S. and S.W.L. are listed as the inventors of several patent applications (62/800,188; 63/174,277; 63/209,941; 63/209,940; 63/209,915; 63/209,924; 17/426,728; 3,128,368; 20748891.7; 2020216486) related to senolytic CAR T cells. M.S. holds other unrelated patents on CAR technologies. C.A. is also an inventor in the patent application 63/510,997. C.A., M.S. and S.W.L. are advisors for Fate Therapeutics. M.S. also receives research support from Fate Therapeutics, is an advisor and has equity in Senecea Therapeutics, and holds other unrelated patents on CAR technologies. S.W.L. is on the scientific advisory board and has equity in ORIC Pharmaceuticals, Blueprint Medicines, Mirimus, Senecea Therapeutics, Faeth Therapeutics and PMV Pharmaceuticals. D.A.T. is a scientific cofounder and scientific advisory board of Mestag Therapeutics and is a member of the Scientific Advisory Board and receives stock options from Leap Therapeutics, Dunad Therapeutics, Cygnal Therapeutics and Mestag Therapeutics outside the submitted work. D.A.T. has received unrelated research grant support from Fibrogen, Mestag and ONO Therapeutics. None of these activities are related to the current publication. R.L.L. is on the supervisory board of Qiagen and is a scientific advisor to Imago, Mission Bio, Zentalis, Ajax, Auron, Prelude, C4 Therapeutics and Isoplexis. R.L.L. receives research support from Ajax, Zentalis and Abbvie and has consulted for Incyte, Janssen and AstraZeneca and has received honoraria from AstraZeneca for invited lectures. L.W.J. owns stock in Pacyclex and Illuminosonics. The other authors declare no competing interests.

Additional information

Extended data is available for this paper at https://doi.org/10.1038/s43587-023-00560-5.

Supplementary information The online version contains supplementary material available at https://doi.org/10.1038/s43587-023-00560-5.

Correspondence and requests for materials should be addressed to Corina Amor.

Peer review information *Nature Aging* thanks Manuel Collado, Ming Xu and the other, anonymous, reviewer(s) for their contribution to the peer review of this work.

Reprints and permissions information is available at www.nature.com/reprints.

Publisher's note Springer Nature remains neutral with regard to jurisdictional claims in published maps and institutional affiliations.

https://doi.org/10.1038/s43587-023-00560-5

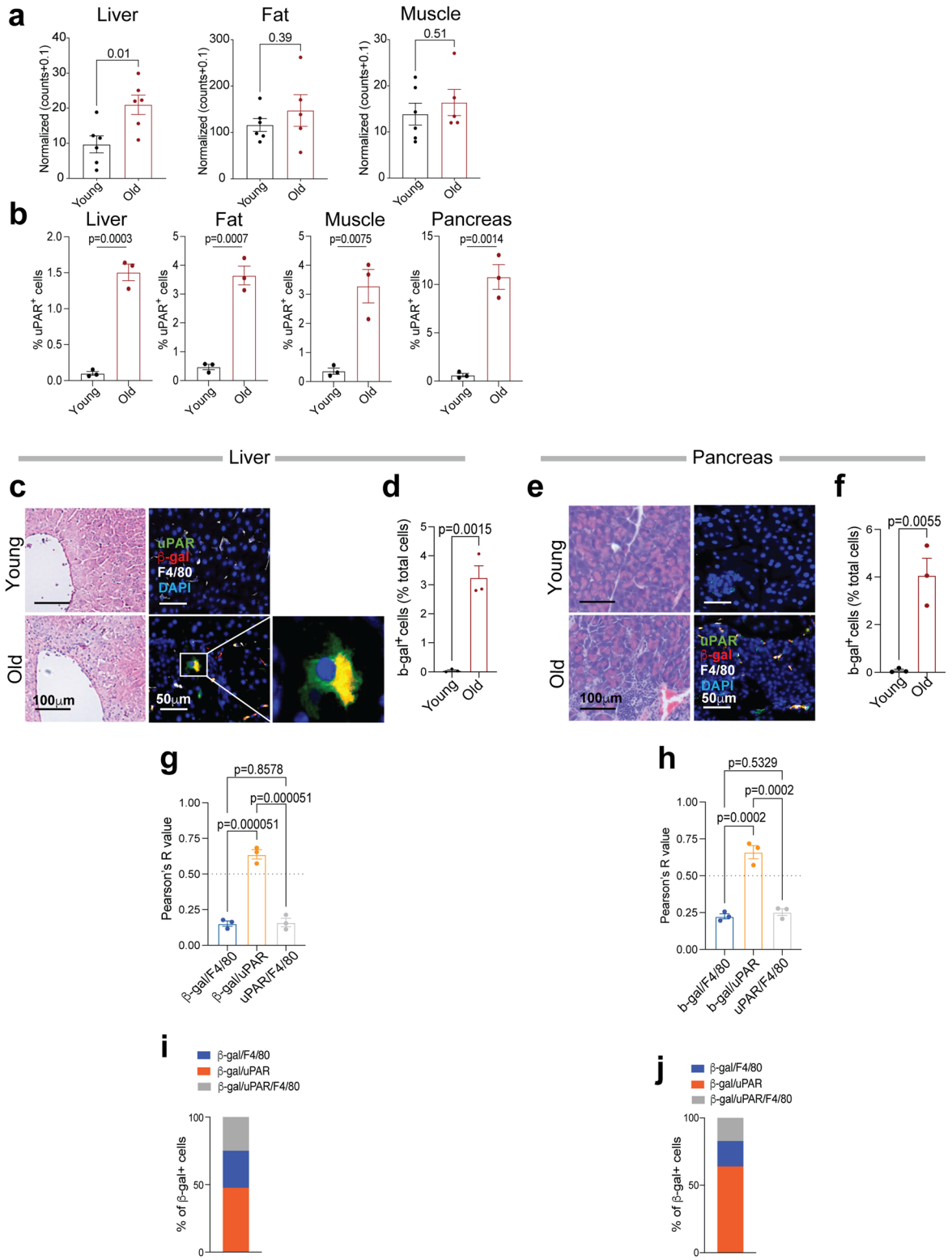

Extended Data Fig. 1 | Characterization of uPAR-positive cells in aging. a, RNA expression of *Plaur* in liver, adipose tissue (fat) and muscle of young (3 months) or old (21 months) mice. Data obtained from the Tabula Muris Senis project[18]. **b**, Quantification of immunohistochemical staining of mouse uPAR in liver, adipose tissue, muscle and pancreas from young (age 3 months) or old (age 20 months) mice (n = 3 per age). **c**, Hematoxylin and eosin staining and immunofluorescence staining of young (age 3 months n = 3 mice) or old (age 18–20 months n = 3 mice) livers. uPAR (green), β-gal (red), F4/80 (white), DAPI (blue). **d**, Percentage of SA-b-gal positive cells in young and aged livers in c. **e**, Hematoxylin and eosin staining and immunofluorescence staining of young (age 3 months n = 3 mice) or old (age 18–20 months n = 3 mice) pancreas. uPAR (green), β-gal (red), F4/80 (white), DAPI (blue). **f**, Percentage of SA-b-gal positive cells in young and aged livers in e. **g,h**, Correlation (Pearson's R value) of β-gal and F4/80 co-staining, β-gal and uPAR co-staining or uPAR and F4/80 co-staining in aged livers (**g**) and aged pancreas (**h**). **i,j**, Percentage of β-gal positive cells that costain for F4/80, uPAR or uPAR and F4/80 in aged livers (**i**) and aged pancreas (**j**). Data are mean ± s.e.m **(a,b,d,f-h);** values are derived from two-tailed unpaired Student's t-tests **(a,b,d,f)** one-way ANOVA with multiple comparisons **(g,h)**. Results are from 1 independent experiment **(a-j)**.

https://doi.org/10.1038/s43587-023-00560-5

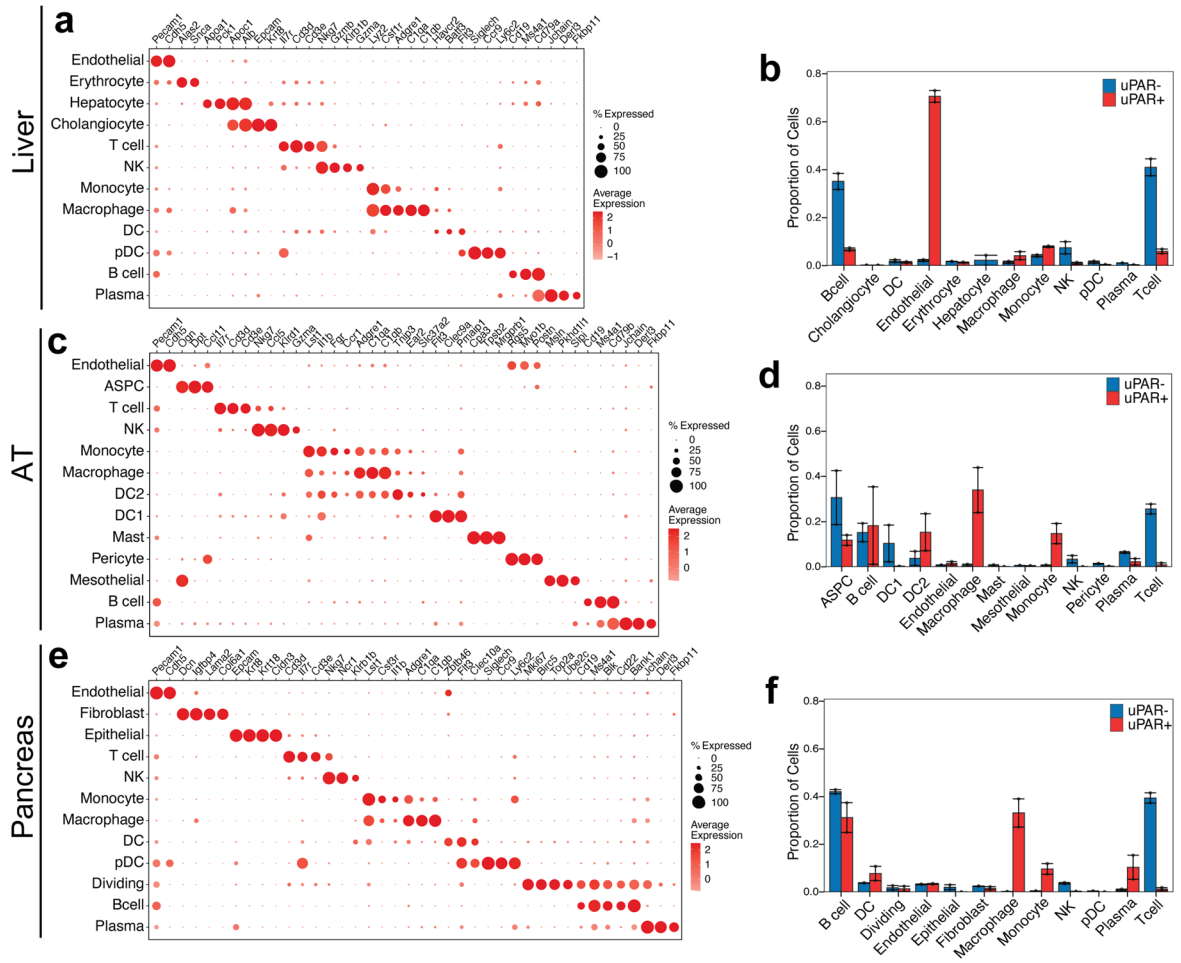

Extended Data Fig. 2 | Single cell profile of aged tissues. a, Dot plot showing expression of 34 signature genes across the 12 lineages of the liver. The size of the dots represents the proportion of cells expressing a particular marker, and the color scale indicates the mean expression levels of the markers (z-score transformed). **b**, Fractions of uPAR-positive and uPAR-negative cells in the various lineages in liver (n= the sequencing of 4 mice where 2 females were combined into one replicate and 2 males were combined into another replicate). Error bars represent s.d. **c**, Dot plot showing expression of 40 signature gene expressions across the 13 lineages of the adipose tissue. The size of the dots represents the proportion of cells expressing a particular marker, and the color scale indicates the mean expression levels of the markers (z-score transformed). **d**, Fractions of uPAR-positive and uPAR-negative cells in the various lineages in adipose tissue (n= the sequencing of 4 mice where 2 females were combined into one replicate and 2 males were combined into another replicate). Error bars represent s.d. **e**, Dot plot showing expression of 40 genes across the 12 lineages of the pancreas. The size of the dots represents the proportion of cells expressing a particular marker, and the color scale indicates the mean expression levels of the markers (z-score transformed). **f**, Fractions of uPAR-positive and uPAR-negative cells in the various lineages in pancreas (n= the sequencing of 4 mice where 2 females were combined into one replicate and 2 males were combined into another replicate). Error bars represent s.d. Data are mean ± s.d.; p values are derived from two-tailed unpaired Student's t-tests **(b,d,f)**. Results are from 1 independent experiment **(a-f)**.

https://doi.org/10.1038/s43587-023-00560-5

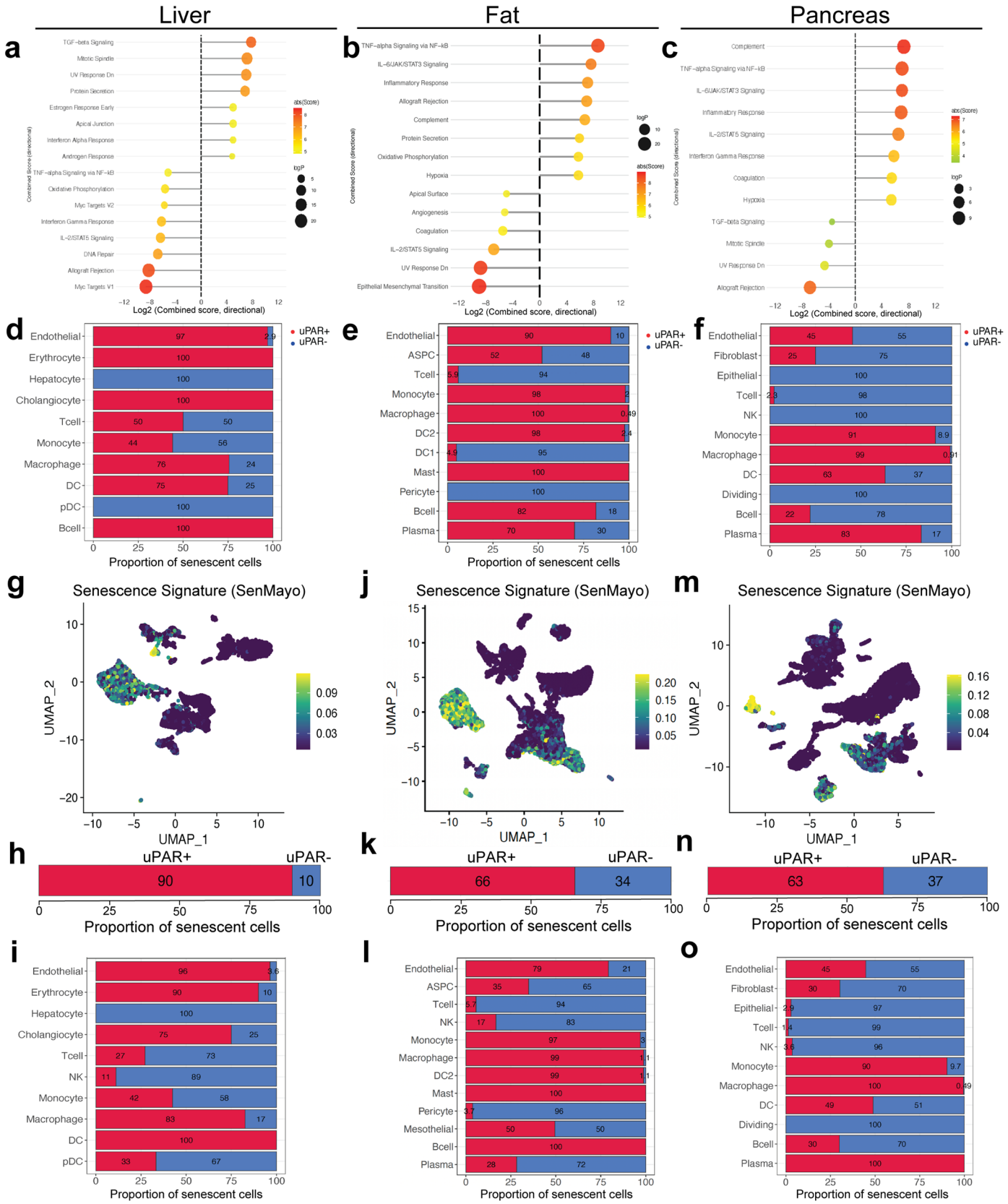

Extended Data Fig. 3 | Characteristics of senescent uPAR-positive cells in aged tissues. a-c, Molecular Signature Database Hallmark 2020 signatures that are significantly enriched in uPAR positive cells vs uPAR negative cells of liver **(a)**, adipose tissue **(b)** and pancreas **(c)**. **d-f**, quantification of the proportion of uPAR positive and negative cells by cell type contributing to the respective senescence signature in Fig. 1h **(d)**, Fig. 1j **(e)** and Fig. 1l **(f)**. **g–o**, UMAP visualizations with senescence signature scores[17] in each cell indicated by the color scale. Below: quantification of the proportion of uPAR positive and negative cells contributing to the respective senescence signature in total **(h,k,n)** and by cell type **(i,l,o)**. **g,h,i**, liver; **j,k,l**, adipose tissue; **m,n,o;** pancreas. Results are from 1 independent experiment with (n = the sequencing of 4 mice where 2 females were combined into one replicate and 2 males were combined into another replicate) **(a-m)**.

https://doi.org/10.1038/s43587-023-00560-5

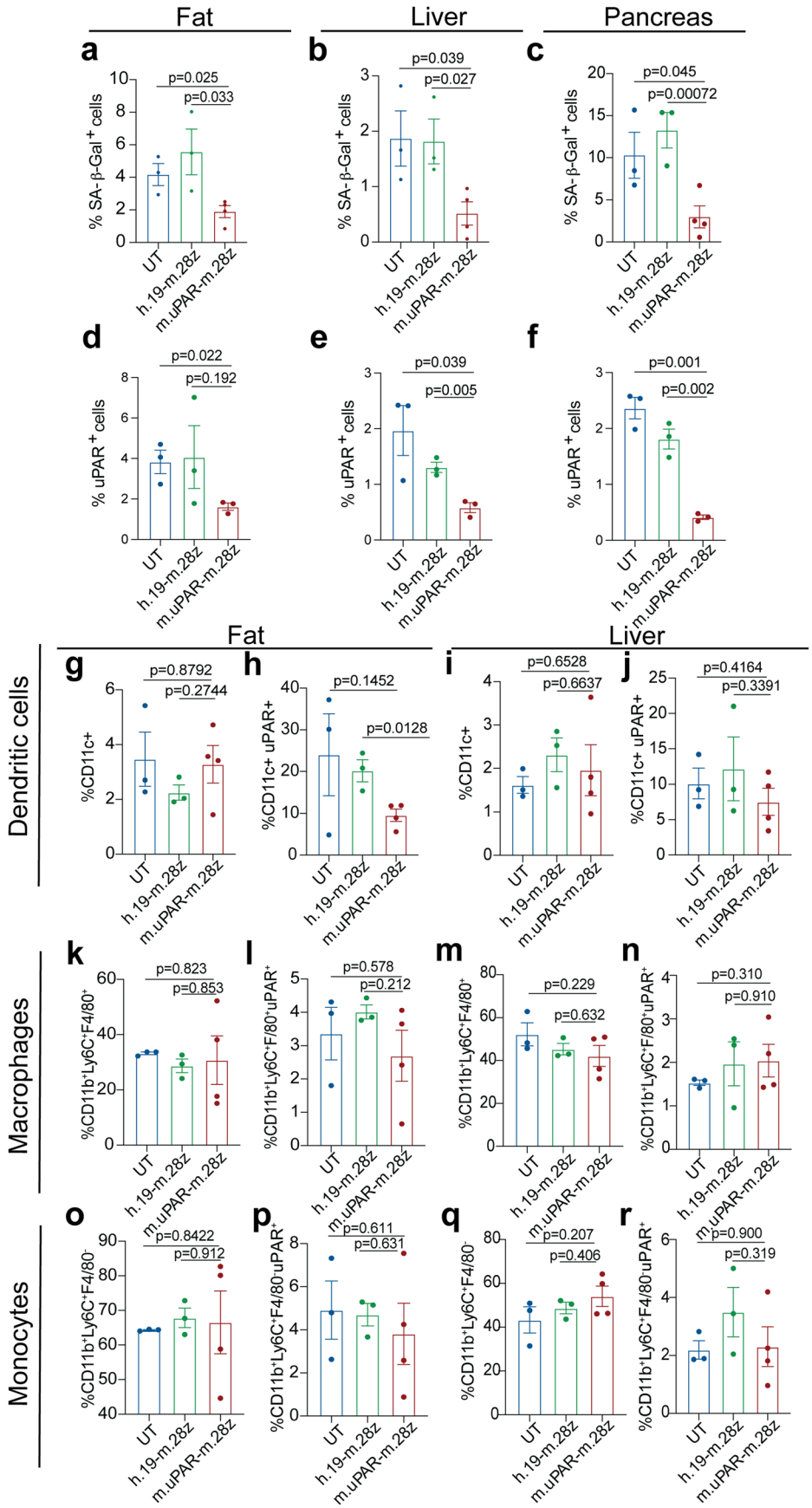

Extended Data Fig. 4 | See next page for caption.

https://doi.org/10.1038/s43587-023-00560-5

Extended Data Fig. 4 | Effect of uPAR CAR T cells on aged tissues. **a-c**, Quantification of SA-β-Gal–positive cells in adipose tissue, liver and pancreas 20 days after cell infusion (n = 3 for UT; n = 3 for h.19-m.28z; n = 4 for m.uPAR-m.28z). **d-f**, Quantification of uPAR-positive cells in adipose tissue, liver and pancreas 20 days after cell infusion (n = 3 per group). **g-j**, Percentage of dendritic cells and uPAR$^+$ dendritic cells in the adipose tissue **(g,h)** or liver **(i,j)** 20 days after cell infusion (n = 3 for UT; n = 3 for h.19-m.28z; n = 4 for m.uPAR-m.28z). **k-n**, Percentage of macrophages and uPAR$^+$ macrophages in the adipose tissue **(k,l,)** or liver **(m,n)** 20 days after cell infusion (n = 3 for UT; n = 3 for h.19-m.28z; n = 4 for m.uPAR-m.28z). **o-r**, Percentage of monocytes and uPAR$^+$ monocytes in the adipose tissue **(o,p)** or liver **(q,r)** 20 days after cell infusion (n = 3 for UT; n = 3 for h.19-m.28z; n = 4 for m.uPAR-m.28z). Results of 1 independent experiment **(a-r)**. Data are mean ± s.e.m.; p values from two-tailed unpaired Student's t-test **(a-r)**.

https://doi.org/10.1038/s43587-023-00560-5

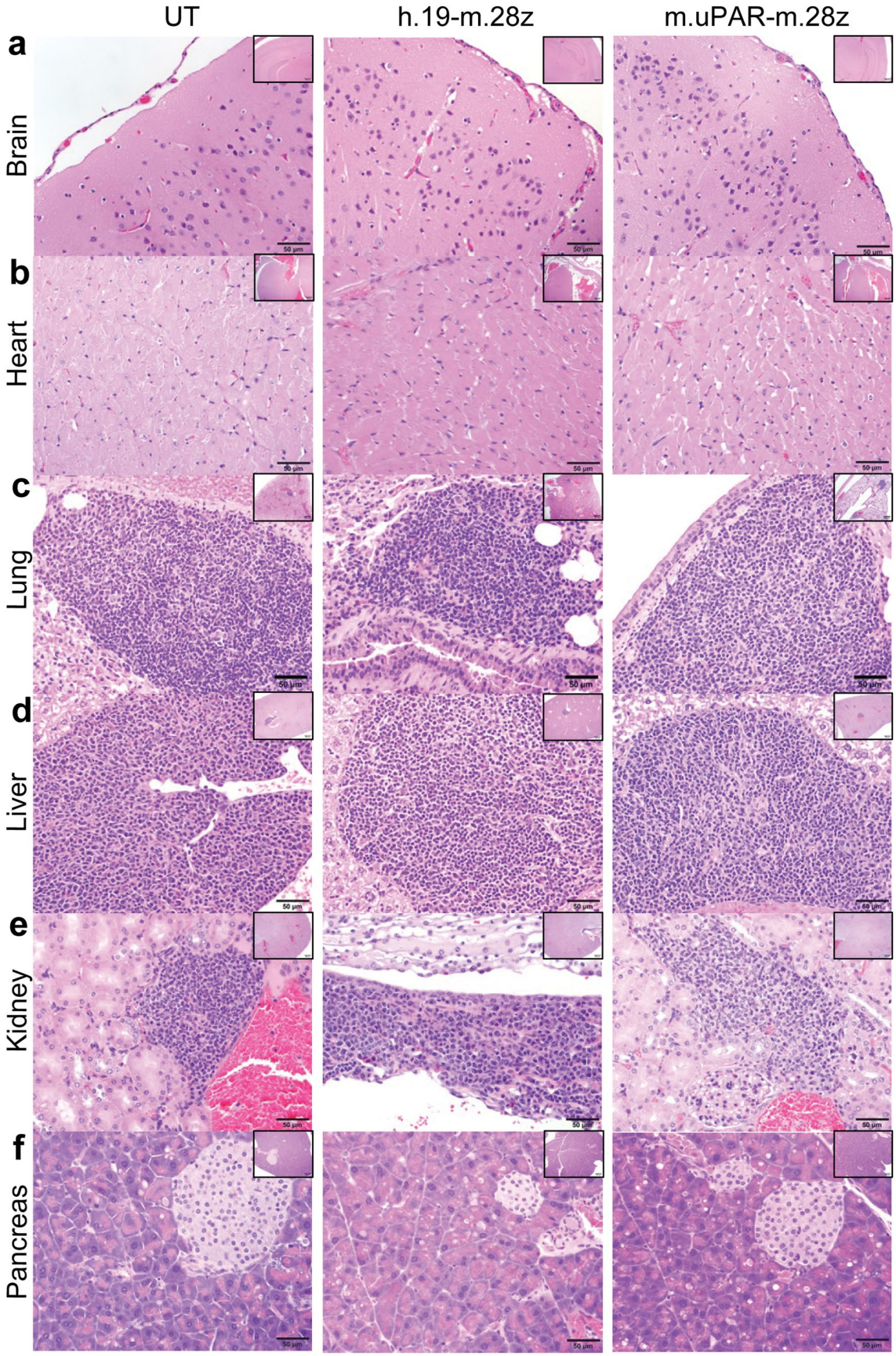

Extended Data Fig. 5 | See next page for caption.

https://doi.org/10.1038/s43587-023-00560-5

Extended Data Fig. 5 | uPAR CAR T cells are not associated with signs of tissue damage in aged tissues and do not exacerbate spontaneous age-related histological changes in lung, liver and kidneys. Mice received cell infusions at 18–20 months and were sacrificed 20 days after infusion of the indicated T cells. Sections were stained with hematoxylin and eosin. Aged mice showed mononuclear leukocytic aggregates composed predominantly of lymphocytes and plasma cells in tissues in an age dependent manner. These leukocytic aggregates were more frequently observed in tissues from uPAR-m.28z CAR T- treated aged mice than tissues from control aged mice and were not associated with necrosis and/or degeneration in tissues from both experimental and control aged mice. These lymphocytic and plasmocytic aggregates in tissues are often observed in naïve aged mice and are considered spontaneous background findings in longitudinal aging studies in mice[50,51]. **a**, Representative sections of normal cerebral cortex and meninges at the level of the posterior hypothalamus (inset: hippocampus). **b**. Histology of normal cardiomyocytes and interstitium in myocardium (inset: ventricles and interventricular septum). **c**. Representative histology of normal lungs showed dense aggregates of lymphocytes and fewer plasma cells and macrophages around bronchioles or vasculature (inset: pulmonary lobes). **d**. The liver from aged mice showed accumulation of lymphocytic and histiocytic aggregates in portal to periportal regions (Inset: hepatic lobe). **e**. Histology of the kidneys showed accumulation of lymphocytes and plasma cells in the renal interstitium (n & o) and around blood vessels (inset: renal cortex, medulla, and pelvis). **f**. Representative sections of normal pancreatic acini (exocrine pancreas) and islets of Langerhans (endocrine pancreas; inset: pancreatic lobule). Images were captured at 4x (insets) and 40x magnifications. Results of 1 independent experiment (with n = 3 per group).

https://doi.org/10.1038/s43587-023-00560-5

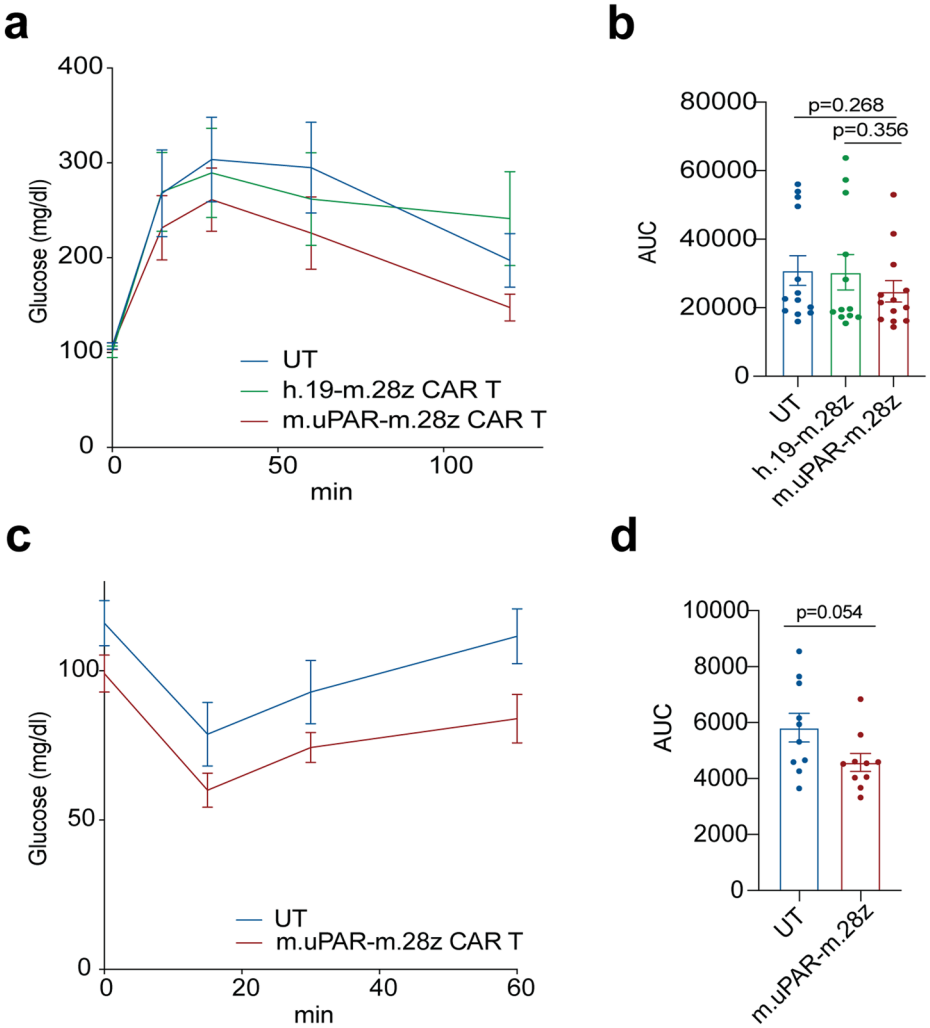

Extended Data Fig. 6 | Effect of uPAR CAR T cells in young and old tissues. **a-b**, Mice received cell infusion at 3 months old. **a**, Levels of glucose before (0 min) and after intraperitoneal administration of glucose (2 g/kg) 2.5 months after cell infusion (n = 13 for untransduced T cells; n = 12 for h.19-m.28z and n = 13 for m.uPAR-m.28z). **b**, Area under the curve (AUC) representing the results from **a**. Each point represents a single mouse. **c-d**, Mice received cell infusion at 18–20 months old. **c**, Levels of glucose before (0 min) and after intraperitoneal administration of insulin (0.5 units/kg body weight) 2.5 months after cell infusion (n = 10 for untransduced T cells and n = 10 for m.uPAR-m.28z). **d**, Area under the curve (AUC) representing the results from **c**. Each point represents a single mouse. Results of 2 independent experiments **(a,b)** or 1 independent experiment **(c,d)**. Data are mean ± s.e.m.; p values from two-tailed unpaired Student's t-test **(b,d)**.

https://doi.org/10.1038/s43587-023-00560-5

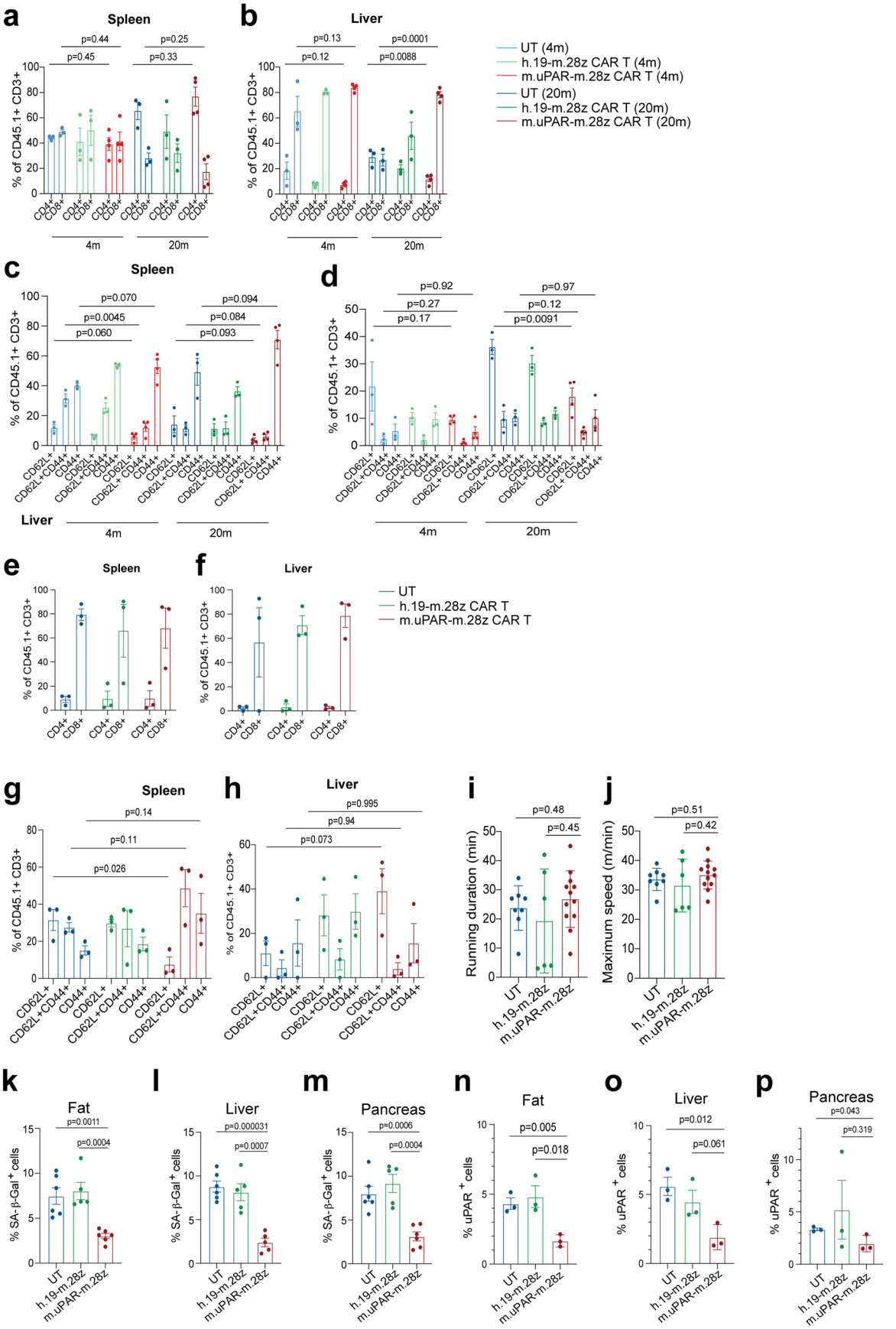

Extended Data Fig. 7 | See next page for caption.

https://doi.org/10.1038/s43587-023-00560-5

Extended Data Fig. 7 | Profile of and long-term effects of uPAR CAR T cells in aging. a,b, Percentage of $CD4^+$ or $CD8^+$ cells among $CD45.1^+$ T cells from the spleen (**a**) or liver (**b**) of 4-month-old or 20-month-old mice 20 days after cell infusion (n = 3 mice per age group for untransduced T cells [UT] and for h.19-m.28z; n = 4 for m.uPAR-m.28z). **c,d**, Percentage of $CD45.1^+$ T cells expressing differentiation markers CD62L and CD44 in the spleen (**c**) or liver (**d**) of 4-month-old or 20-month-old mice 20 days after cell infusion (sample sizes as in **a**). **e,f**, Percentage of $CD4^+$ or $CD8^+$ cells among $CD45.1^+$ T cells in the spleen (**e**) or liver (**f**) of 15-month-old mice 12 months after cell infusion (n = 3 mice per group). **g,h**, Percentage of $CD45.1^+$ T cells expressing differentiation markers CD62L and CD44 on $CD45.1^+$ T cells in the spleen (**g**) or liver (**h**) of 15-month-old mice 12 months after cell infusion (n = 3 mice per group). **i**, Time to exhaustion in exercise capacity testing 12 months after cell infusion (n = 8 for untransduced T cells; n = 6 for h.19-m.28z; n = 12 for m.uPAR-m.28z). **j**, Maximum speed (m/min) in capacity testing 12 months after cell infusion (sample sizes as in **i**). **k-m**, Quantification of SA-β-Gal–positive cells 12 months after cell infusion in **(k)** adipose tissue (n = 6 for UT; n = 5 for h.19-m.28z; n = 6 for m.uPAR-m.28z); **(l)** liver (n = 6 for UT; n = 5 for h.19-m.28z; n = 5 for m.uPAR-m.28z) and **(m)** pancreas (n = 6 for UT; n = 5 for h.19-m.28z; n = 6 for m.uPAR-m.28z). **n-p**, Quantification of uPAR-positive cells in **(n)** adipose tissue, **(o)** liver and **(p)** pancreas 12 months after cell infusion (n = 3 per group). Results of 1 independent experiment **(a-h, n-p)** or 2 independent experiments **(i-m)**. Data are mean ± s.e.m.; p values from two-tailed unpaired Student's t-test **(a-h, k-p)** or two-tailed Mann Whitney test **(i,j)**.

https://doi.org/10.1038/s43587-023-00560-5

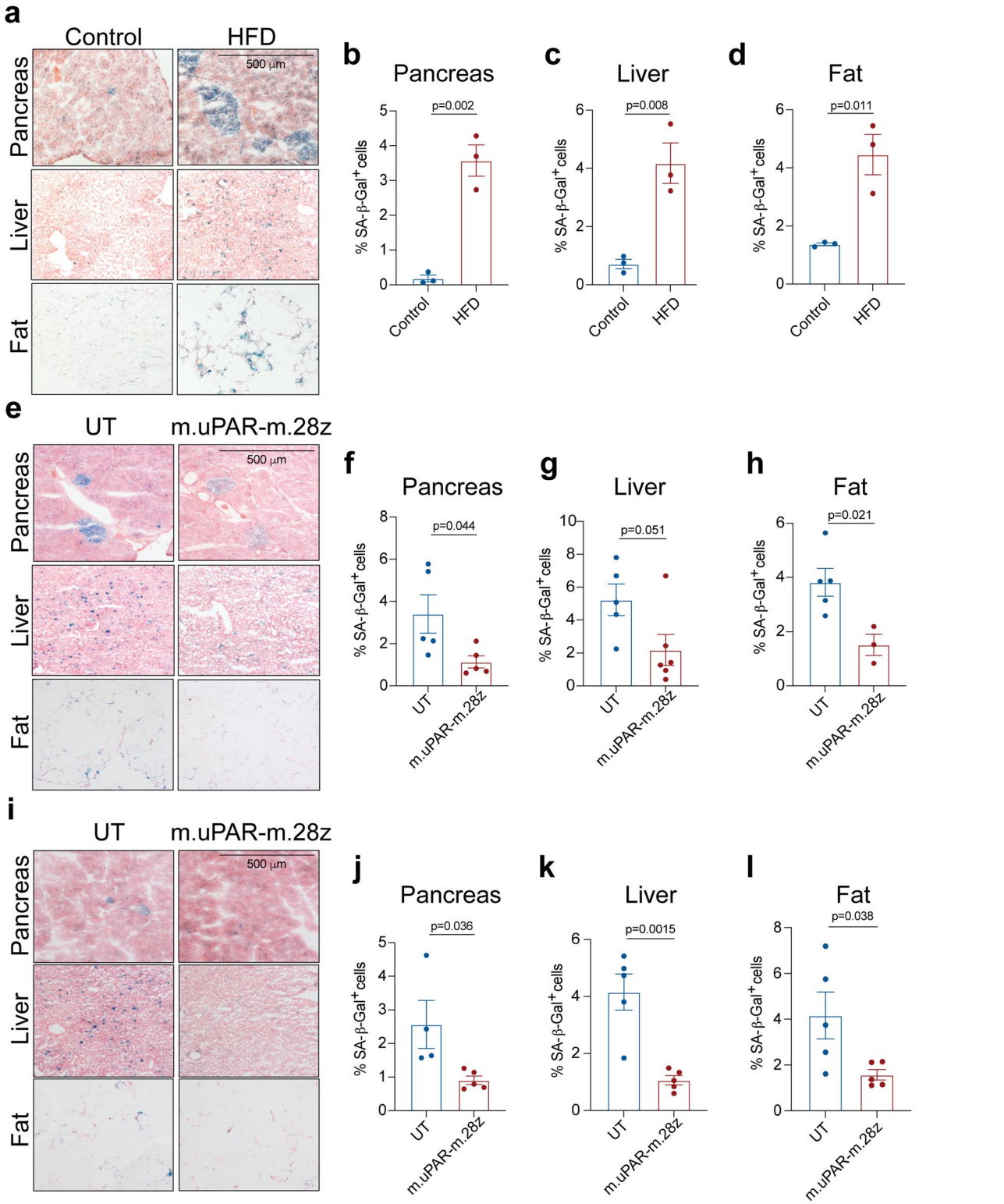

Extended Data Fig. 8 | uPAR CAR T cells decrease senescent cell burden in therapeutic and preventive settings in high fat diet. a, Representative staining of SA-β-Gal after two months of high fat diet or normal chow diet. **b-d;** Quantification of SA-β-Gal–positive cells in pancreas, liver and adipose tissue after two months of high fat diet or normal chow diet (n = 3 for chow; n = 3 HFD). **e**, Representative staining of SA-β-Gal 1 month after cell infusion in the experimental scheme depicted in Fig. 7a. **f-h;** Quantification of SA-β-Gal–positive cells in pancreas, liver and adipose tissue 1 month after cell infusion (n = 5 for UT; for m.uPAR-m.28z n = 5 in pancreas, n = 6 in liver and n = 3 in adipose tissue). UT, untransduced T cells. **i**, Representative staining of SA-β-Gal 3.5 months after cell infusion in the experimental scheme depicted in Fig. 7j. **j-l**, Quantification of SA-β-Gal–positive cells in pancreas, liver, and adipose tissue 3.5 months after cell infusion (UT n = 4 in pancreas, n = 5 in liver and adipose tissue; for m.uPAR-m.28z n = 5). Each panel shows results from 1 experiment. Data are mean ± s.e.m.; p values from two-tailed unpaired Student's t-test **(b-d; f-h; j-l)**.

https://doi.org/10.1038/s43587-023-00560-5

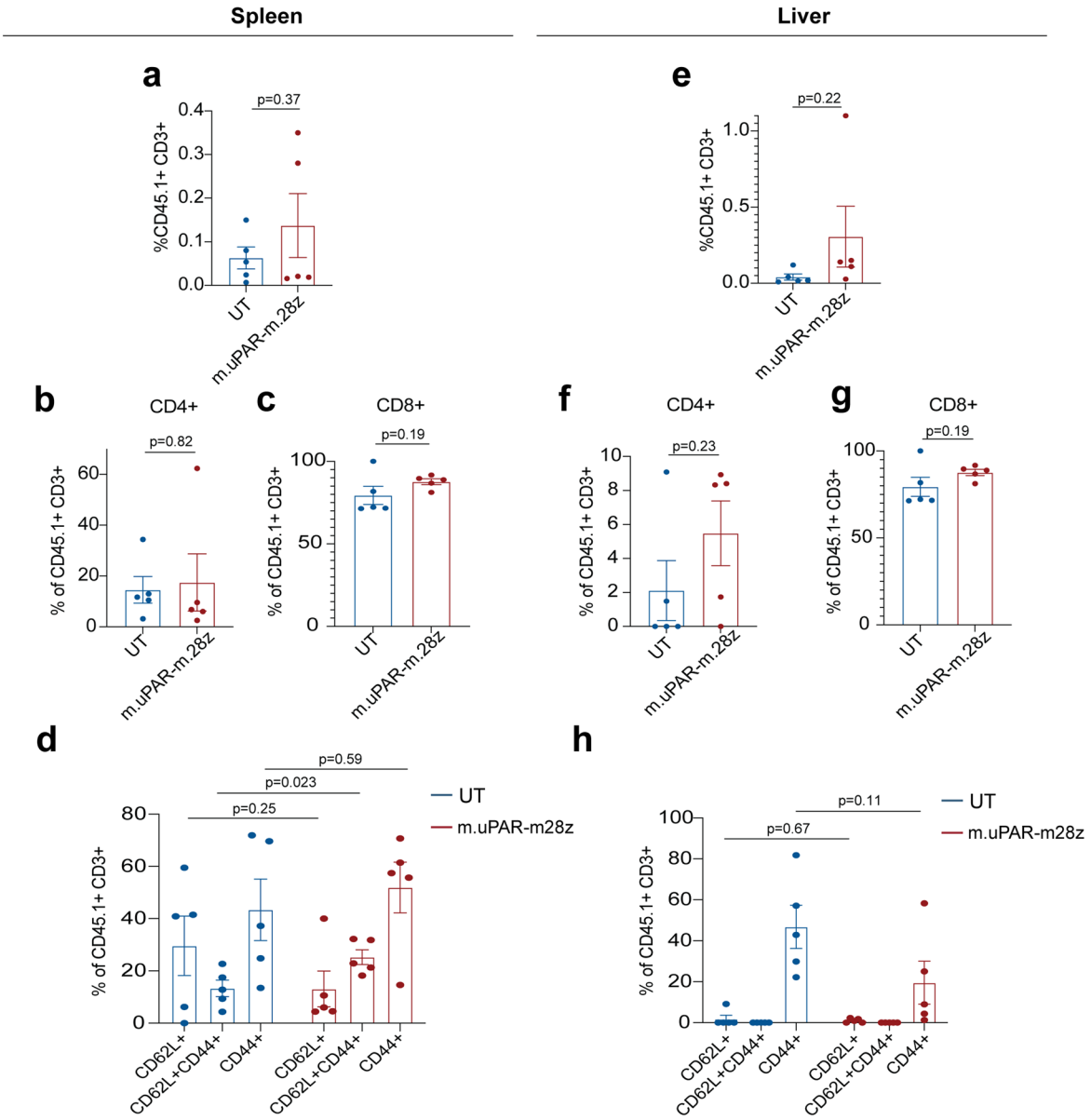

Extended Data Fig. 9 | Profile and persistence of uPAR CAR T cells in metabolic syndrome. T cells were assessed in spleen (**a**-**d**) and liver (**e**-**h**) 3.5 months after cell infusion in the experimental scheme depicted in Fig. 7j. **a**, Percentage of CD45.1$^+$ T cells in the spleen. **b**, Percentage of CD4$^+$ cells among CD45.1$^+$ T cells in the spleen. **c**, Percentage of CD8$^+$ cells among CD45.1$^+$ T cells in the spleen. **d**, Percentage of CD45.1$^+$ T cells from the spleen expressing differentiation markers CD62L and CD44. **e**, Percentage of CD45.1$^+$ T cells in the liver. **f**, Percentage of CD4$^+$ cells among CD45.1$^+$ T cells in the liver. **g**, Percentage of CD8$^+$ cells among CD45.1$^+$ T cells in the liver. **h**, Percentage of CD45.1$^+$ T cells in the liver expressing differentiation markers CD62L and CD44. Results in each panel are from 1 experiment (n = 5 mice per group). Data are mean ± s.e.m.; p values from two-tailed unpaired Student's t-test.

https://doi.org/10.1038/s43587-023-00560-5

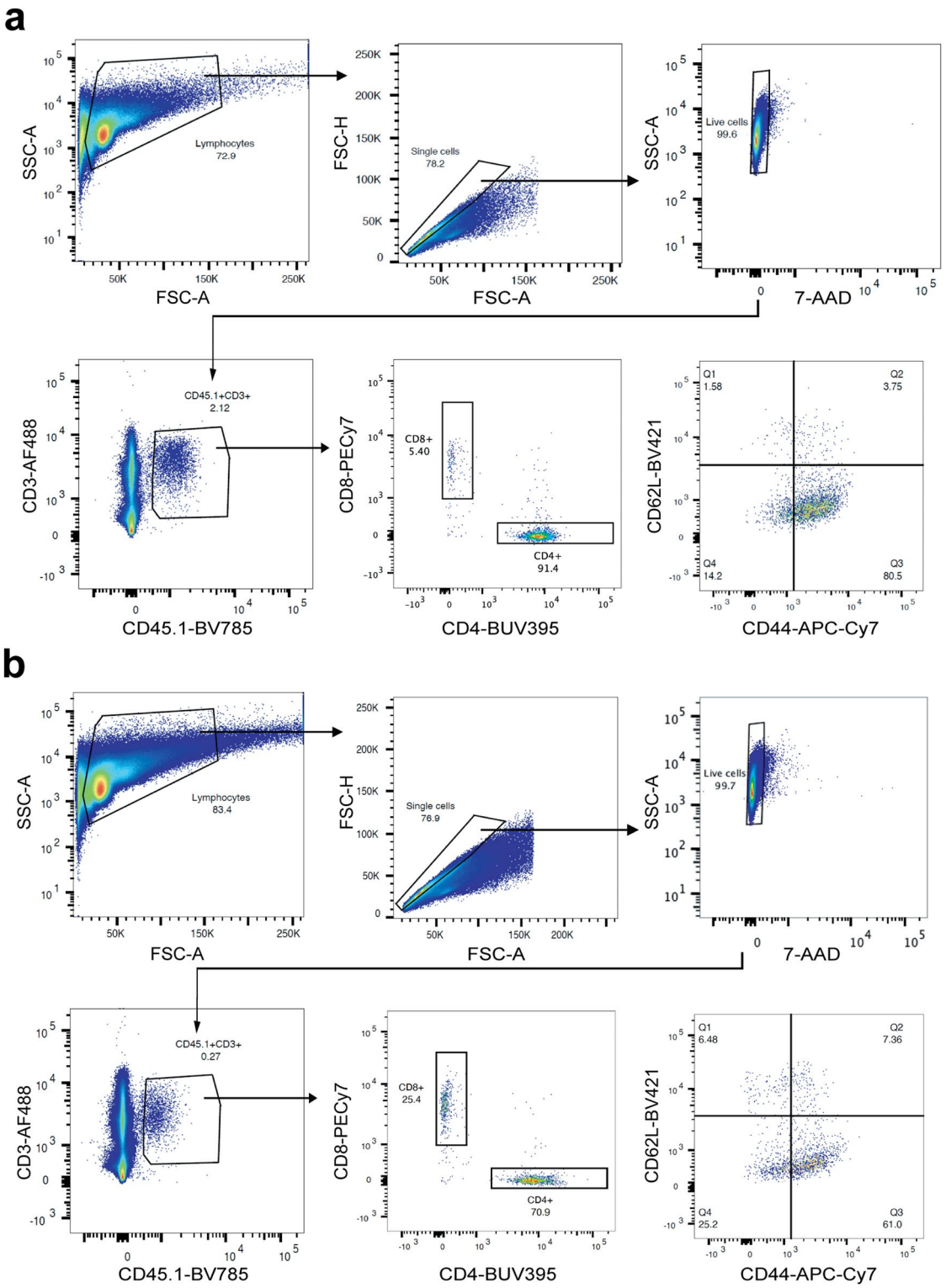

Extended Data Fig. 10 | Gating strategies. a,b, Representative flow cytometry staining of m.uPAR-m.28z **(a)** or untransduced T cells **(b)** obtained from the spleens of mice 20 days after cell infusion as depicted in Fig. 5g. Shown are results of 1 independent experiment (n = 3 mice for untransduced T cells; n = 4 mice for m.uPAR-m.28z).

nature portfolio

Corresponding author(s): Corina Amor Vegas

Last updated by author(s): Dec 11, 2023

Reporting Summary

Nature Portfolio wishes to improve the reproducibility of the work that we publish. This form provides structure for consistency and transparency in reporting. For further information on Nature Portfolio policies, see our Editorial Policies and the Editorial Policy Checklist.

Statistics

For all statistical analyses, confirm that the following items are present in the figure legend, table legend, main text, or Methods section.

n/a	Confirmed
☐	☒ The exact sample size (*n*) for each experimental group/condition, given as a discrete number and unit of measurement
☐	☒ A statement on whether measurements were taken from distinct samples or whether the same sample was measured repeatedly
☐	☒ The statistical test(s) used AND whether they are one- or two-sided *Only common tests should be described solely by name; describe more complex techniques in the Methods section.*
☒	☐ A description of all covariates tested
☐	☒ A description of any assumptions or corrections, such as tests of normality and adjustment for multiple comparisons
☐	☒ A full description of the statistical parameters including central tendency (e.g. means) or other basic estimates (e.g. regression coefficient) AND variation (e.g. standard deviation) or associated estimates of uncertainty (e.g. confidence intervals)
☐	☒ For null hypothesis testing, the test statistic (e.g. *F*, *t*, *r*) with confidence intervals, effect sizes, degrees of freedom and *P* value noted *Give P values as exact values whenever suitable.*
☒	☐ For Bayesian analysis, information on the choice of priors and Markov chain Monte Carlo settings
☒	☐ For hierarchical and complex designs, identification of the appropriate level for tests and full reporting of outcomes
☐	☒ Estimates of effect sizes (e.g. Cohen's *d*, Pearson's *r*), indicating how they were calculated

Our web collection on statistics for biologists contains articles on many of the points above.

Software and code

Policy information about availability of computer code

Data collection	BD-Fortessa cytometer, SONY SH800S sorter, ZEISS Axio Observer microscopy, BX45 microscope, 10X Genomics' Cell Ranger software v7.1.0, IDEXX Procyte DX, Beckman Coulter AU680 analyzer, Microsoft Excel for Mac.
Data analysis	FlowJo 10.8.1, GraphPad Prism V.9.3.1, Fiji-ImageJ v2.1.051

For manuscripts utilizing custom algorithms or software that are central to the research but not yet described in published literature, software must be made available to editors and reviewers. We strongly encourage code deposition in a community repository (e.g. GitHub). See the Nature Portfolio guidelines for submitting code & software for further information.

Data

Policy information about availability of data

All manuscripts must include a data availability statement. This statement should provide the following information, where applicable:

- Accession codes, unique identifiers, or web links for publicly available datasets
- A description of any restrictions on data availability
- For clinical datasets or third party data, please ensure that the statement adheres to our policy

Source data is provided with this paper. scRNA-seq data presented in this study is deposited in the Gene Expression Omnibus (GEO) database under accession number GSE243616. Data from the Tabula Muris Senis project18 was accessed through https://twc-stanford.shinyapps.io/maca/. Human dataset from26 was

accessed through https://zenodo.org/records/7311202#.Y20ybezMlyI. Requests for materials should be addressed to the corresponding authors.
All code is available at https://github.com/naikai/Amor_et_al_2023

Human research participants

Policy information about studies involving human research participants and Sex and Gender in Research.

Reporting on sex and gender	Not applicable
Population characteristics	Not applicable
Recruitment	Not applicable
Ethics oversight	Not applicable

Note that full information on the approval of the study protocol must also be provided in the manuscript.

Field-specific reporting

Please select the one below that is the best fit for your research. If you are not sure, read the appropriate sections before making your selection.

☒ Life sciences ☐ Behavioural & social sciences ☐ Ecological, evolutionary & environmental sciences

For a reference copy of the document with all sections, see nature.com/documents/nr-reporting-summary-flat.pdf

Life sciences study design

All studies must disclose on these points even when the disclosure is negative.

Sample size	No statistical methods were used to pre-determine sample size. Sample sizes were estimated based on preliminary experiments, with an effort to achieve a minimum of n=3 mice per treatment group which proved to be sufficient to reproducibly observe a statistical significant difference. For statistical testing we did not include adjustment for multiple comparisons. The rationale for this is that , two control groups were compared to the experimental group, but it could have been biologically possible to just have one control group. Thus, for any given endpoint, there were two pairwise comparisons: the experiment group separately compared to each control. While two tests were evaluated, we only considered the analysis statistically significant if both tests had a p-value less than 0.05. If only one of the two tests was significant, we did not claim the groups were significantly different; instead, we considered the analysis inconclusive and reported a trend. Viewing the analysis as significant only if both p-values were less than 0.05 preserves the family-wise error rate at less than 0.05. Therefore, there is no need to further adjust for multiple comparisons.
Data exclusions	No data was excluded. For histological assesment of HFD experiments OCT cassettes of samples containing adipose tissue or pancreas that were folded and presented a morphology that did not allowed for successful slide generation were not further processed.
Replication	All experiments were repeated in replicates and/or from different subjects in independent experiments. All attempts at replication were successful. Information for replication of each experiment is included in the figure legends.
Randomization	Mice were randomly assigned into treatment groups ensuring equal sex distribution among groups.
Blinding	Mouse conditions were observed by an operator who was blinded to the treatment groups in addition to the main investigator who was not blind to group allocation. Pathological analysis and exercise testing studies were performed in a blinded fashion. Data analysis was not performed in a blinded fashion. Data analysis are based on objectively measurable data (cell count, blood tests).

Reporting for specific materials, systems and methods

We require information from authors about some types of materials, experimental systems and methods used in many studies. Here, indicate whether each material, system or method listed is relevant to your study. If you are not sure if a list item applies to your research, read the appropriate section before selecting a response.

Materials & experimental systems

n/a	Involved in the study
☐	☒ Antibodies
☒	☐ Eukaryotic cell lines
☒	☐ Palaeontology and archaeology
☐	☒ Animals and other organisms
☒	☐ Clinical data
☒	☐ Dual use research of concern

Methods

n/a	Involved in the study
☒	☐ ChIP-seq
☐	☒ Flow cytometry
☒	☐ MRI-based neuroimaging

Antibodies

Antibodies used

The following fluorophore-conjugated antibodies were used in the indicated dilutions: Myc-tag AF647 (clone 9B11, Cell Signaling Technology, 2233S, lot 25, 1:50), m.CD45.1 BV785 (clone A20, Biolegend, 110743, lot B347719, 1:100), m.CD45.2 BV785 (clone 104, Biolegend, 109839, lot B343292, 1:100), mCD3 AF488 (clone 17A2, Biolegend, 100210, lot B284975, 1:100), mCD4 BUV395 (clone GK1.5, BD, 563790, lot 1097734, 1:50), mCD8 PE-Cy7 (clone 53-6.7, Biolegend, 100722, lot B312604, 1:50), mCD62L BV421 (clone MEL-14, Biolegend, 104435, lot B283191, 1:50), mCD44 APC Cy7 (clone IM7, BD Pharminogen, 560568, lot 1083068, 1:100), mCD3 BV650 (clone 17A2, Biolegend, 100229, lot B350667, 1:100),mCD19 BV650 (clone1D3, BD Biosciences, 563235, lot 1354015 1:100), mNKp46 BV650 (clone 29A1.4, Biolegend, 137635, lot B298809 1:100), mCD11b BUV395 (clone M1/70, BD Biosciences, 563553, lot 0030272 1:50), mLy-6C APC-Cy7 (clone HK1.4, Biolegend, 128026, lot B375238 1:100), mly6G BV605 (clone 1A8, BD Biosciences, 563005, lot2144780 1:100), m.uPAR AF700 (R&D systems, FAB531N, lot 1656339, 1:50), m.uPAR PE (R&D systems, FAB531P, lot ABLH0722051, 1:50), mF4/80 PE-eFluor610 (Clone BM8, Invitrogen, 61-4801-82, lot 2338698, 1:100). uPAR (AF534,R&D lot DCL0521042, 1:50), F4/80 (CI:A3-1, BioRad, Lot 155529, 1:100), anti-Horse anti-goat IgG (30116; Vector Laboratories, lot ZH0526). 7-AAD (BD, 559925, lot 9031655, 1:40) or Ghost UV 450 Viability Dye (13-0868-T100, Tonbo Biosciences lot D0868083018133, 1ul/ml) was used as viability dye.

Validation

All used antibodies were titrated. All the antibodies are validated for use in flow cytometry or immunohistochemistry or immunofluorescence. Data are available at the manufacturer's website. All used antibodies are commercially available. The following antibodies have been validated by the manufacturer against the mentioned species: Myc-tag AF647 (clone 9B11, Cell Signaling Technology, 2233S, lot 25, 1:50 all species), m.CD45.1 BV785 (clone A20, Biolegend, 110743, lot B347719, 1:100, mouse), m.CD45.2 BV785 (clone 104, Biolegend, 109839, lot B343292, 1:100, mouse), mCD3 AF488 (clone 17A2, Biolegend, 100210, lot B284975, 1:100, mouse), mCD4 BUV395 (clone GK1.5, BD, 563790, lot 1097734, 1:50, mouse), mCD8 PE-Cy7 (clone 53-6.7, Biolegend, 100722, lot B312604, 1:50, mouse), mCD62L BV421 (clone MEL-14, Biolegend, 104435, lot B283191, 1:50, mouse), mCD44 APC Cy7 (clone IM7, BD Pharminogen, 560568, lot 1083068, 1:100, mouse), mCD3 BV650 (clone 17A2, Biolegend, 100229, lot B350667, 1:100,mouse),mCD19 BV650 (clone1D3, BD Biosciences, 563235, lot 1354015 1:100,mouse), mNKp46 BV650 (clone 29A1.4, Biolegend, 137635, lot B298809 1:100,mouse), mCD11b BUV395 (clone M1/70, BD Biosciences, 563553, lot 0030272 1:50,mouse), mLy-6C APC-Cy7 (clone HK1.4, Biolegend, 128026, lot B375238 1:100,mouse), mly6G BV605 (clone 1A8, BD Biosciences, 563005, lot2144780 1:100,mouse), m.uPAR AF700 (R&D systems, FAB531N, lot 1656339, 1:50, mouse), m.uPAR PE (R&D systems, FAB531P, lot ABLH0722051, 1:50,mouse), mF4/80 PE-eFluor610 (Clone BM8, Invitrogen, 61-4801-82, lot 2338698, 1:100,mouse). uPAR (AF534,R&D lot DCL0521042, 1:50,mouse), F4/80 (CI:A3-1, BioRad, Lot 155529, 1:100,mouse), anti-Horse anti-goat IgG (30116; Vector Laboratories, lot ZH0526, mouse).

Animals and other research organisms

Policy information about studies involving animals; ARRIVE guidelines recommended for reporting animal research, and Sex and Gender in Research

Laboratory animals

The following mice were used: 3- to 4-month-old C57BL/6 mice (purchased from Charles River), 18-20-month-old C57BL/6 mice (obtained from the National Institute of Aging or the Jackson Laboratory), and 6-week-old B6.SJL-Ptrca/BoyAiTac (CD45.1 mice) (purchased from Taconic). Mice of both sexes were used at 8-12 weeks of age and 18-20 months of age for the aging experiment, males of 8-12 weeks for the high fat diet experiments and females of 6-10 weeks old for T cell isolation. Mice were maintained under specific pathogen-free conditions. Housing was on a 12h-12h light-dark cycle under standard temperature and humidity of approximately 18-24C and 40-60%, respectively. Mice were kept in group housing. Mice had free access to food and water except during the starvation period before glucose or insulin tolerance testing. Aging mice were fed a normal diet (PicoLab Rodent Diet 20, LabDiet), mice on the high fat diet (HFD) experiments were fed a HFD (TD.06414, 60% of kcal from fat; Envigo).

Wild animals

This study did not involve wild animals.

Reporting on sex

Mice of both sexes were used at 8-12 weeks of age and 18-20 months of age for the aging experiment, males of 8-12 weeks for the high fat diet experiments and females of 6-10 weeks old for T cell isolation.

Field-collected samples

This study did not involve samples collected from the field.

Ethics oversight

Memorial Sloan Kettering Cancer Center (MSKCC) and Cold Spring Harbor Laboratory (CSHL) Internal Animal Care and Use Committee (animal protocol 11-06-011 at MSKCC and 21-4 at CSHL).

Note that full information on the approval of the study protocol must also be provided in the manuscript.

Flow Cytometry

Plots

Confirm that:

☒ The axis labels state the marker and fluorochrome used (e.g. CD4-FITC).

☒ The axis scales are clearly visible. Include numbers along axes only for bottom left plot of group (a 'group' is an analysis of identical markers).

☒ All plots are contour plots with outliers or pseudocolor plots.

☒ A numerical value for number of cells or percentage (with statistics) is provided.

Methodology

Sample preparation	Livers were dissociated using the MACS liver dissociation kit (Miltenyi Biotec, 130-1-5-807), filtered through a 100-µm strainer and washed with PBS, and red blood cells were lysed by an ACK (ammonium–chloride–potassium) lysing buffer (Lonza). Cells were washed with PBS, resuspended in FACS buffer and either used for immediate analysis or fixed with Fixation Buffer (BD Biosciences; 554655) according to the manufacturer's instructions and used for later analysis. Spleens were mechanically disrupted with the back of a 5-ml syringe, filtered through a 40-µm strainer and washed with PBS and 2 mM EDTA, then red blood cells were lysed by ACK lysing buffer (Lonza). Cells were washed with PBS and 2 mM EDTA, resuspended in FACS buffer and either used for immediate analysis or fixed with Fixation Buffer (BD Biosciences;554655) and used for later analysis. Gonadal adipose tissue was dissociated as described43. In short, adipose tissue was isolated and placed in a digestion solution consisting of 4 mg/ml collagenase, type II (Sigma) in DPBS (Life Technologies) supplemented with 0.5% BSA (Sigma) and 10 mM CaCl2 digested at 37° C for 20 min in a rotational shaker (200 rpm). Afterwards, samples were mechanically dissociated with a 10-ml serological pipette, filtered through a 40-µm strainer and washed with PBS and 2 mM EDTA, then red blood cells were lysed by ACK lysing buffer (Lonza). Pancreata were placed into cold DMEM with 10% FBS and penicillin and streptomycin. The pancreata were minced in this media on ice into 2- to 4-mm fragments so that they would pass through the end of 1-ml pipette tip with ease. The minced tissue was collected in a 15-ml Falcon tube and dissociated in 100 mg/ml Dispase (Life Tech., cat. 17105041), 20 mg/ml collagenase P (Roche, cat. 11249002001) and 1 mM EDTA for 20 minutes on a heated rocker at 37° C (Eppendorf). After 20 minutes, 5 ml of DMEM with 10% FBS was added to quench the reaction. The supernatant was removed and filtered through a 100-µm filter(VWR). Next, 5 ml of dissociation media consisting of 100 mg/ml Dispase (Life Tech., cat. 17105041), 20 mg/ml collagenase P (Roche, cat. 11249002001) and 1 mM EDTA was added prior to replacing the 15-ml tube into the heated rocker for 20 minutes. The reaction was quenched again after 20 minutes with media and filtered via a 100-µm filter. The dissociated cells were spun at 500 rcf for 10 minutes in a swinging bucket centrifuge. The supernatant was discarded and the cells were resuspended in ACK lysis buffer for 2-4 minutes in ice. Cells were washed with PBS, resuspended in FACS buffer and either used for immediate analysis or fixed with Fixation Buffer (BD Biosciences;554655) and used for later analysis.
Instrument	Fortessa 3,BD.
Software	Collection: FACS DIVA. Analysis: Flowjo 10.1
Cell population abundance	The purity was verified by flow cytometry.
Gating strategy	The starting cell population was gated on a SSC-A/FSC-A plot. Cell siglets were identified by FSC/SSC gating. Positive/Negative populations were determined by FMO controls.

☒ Tick this box to confirm that a figure exemplifying the gating strategy is provided in the Supplementary Information.